STOCHASTIC MODELING OF FLOW BEHAVIOR AND CELL STRUCTURE FORMATION DURING EXTRUSION OF BIOPOLYMER MELTS

by

PAVAN HARSHIT MANEPALLI

B.Tech, Indian Institute of Technology, Kharagpur, 2012

A THESIS

submitted in partial fulfillment of the requirements for the degree

MASTER OF SCIENCE

Department of Grain Science and Industry
College of Agriculture

KANSAS STATE UNIVERSITY
Manhattan, Kansas

2014

Approved by:

Major Professor
Dr. Sajid Alavi

Copyright

Abstract

Extrusion is a widely used processing technology for various food products and is also commonly applied in non-food applications involving plastics, rubber and metal. Expanded products for human and animal consumption such as snacks, breakfast cereal, pet food and aquatic food typically consist of a biopolymer matrix of starch and proteins that have natural physical, chemical and polymeric variability. Additionally, variability in extrusion parameters such as water injection and screw speed is often observed depending on the process controls employed. This can potentially lead to inconsistency in product quality. Stochastic modeling helps in studying the impact of variability of various parameters on the end product, which in turn helps in better process and product quality control. The primary purpose of this research was to develop a mathematical model for flow behavior of biopolymer melts inside extruder barrel and bubble growth dynamics after exiting the extruder using mass, heat and momentum transfer equations. This model was integrated with a Monte-Carlo based stochastic interface for input of randomly generated process data (based on experimental data acquisition) and output of simulated distributions of end-product properties such as expansion ratio and cellular architecture parameters (cell size and wall thickness).

The mathematical model was experimentally validated using pilot-scale twin screw extrusion for processing of cereal-based cellular products. Process and product data were measured at different in-barrel moisture contents (19-28% dry basis) and experimental screw speeds (250-330 rpm). Experimental process parameters such as specific mechanical energy (212.8-319.3 kJ/kg), die temperature (120.7-170.6^{o}C), die pressure (3160-7683 kPa) and product characteristics such as expansion ratio (3.29-16.94) and cell size or bubble radius (435-655 microns) compared well with simulated results from the mathematical model viz., specific

mechanical energy (217.6-323.9 kJ/kg), die temperature (116.8-176.1^{o}C), die pressure (3478-6404 kPa), expansion ratio (4.56-19.4) and bubble radius (426-728 microns). Experimental variability in product characteristics was quantified using coefficient of variation which compared well with simulation results (example, 2.5-4.9% versus 0.24-3.1% respectively for expansion ratio). The stochastic model was also used to conduct sensitivity analysis for understanding which raw material and process characteristics contribute most to product variability. Sensitivity analysis showed that the water added in extruder affects the magnitude and variability of expansion ratio the most, as compared to screw speed and consistency index.

Contents

List of Figures

List of Tables

Acknowledgements

I am very grateful to Dr. Sajid Alavi for giving me this opportunity for pursuing Masters at Kansas State University. He has been my mentor and his motivation and guidance has boosted my thirst for knowledge. I am very much influenced by his scientific knowledge and dedication.

I would like to thank my committee members: Dr. Hulya Dogan and Dr. John Mathew for their support and help that set directions of focus throughout my project. I want to thank Eric Maichel, Max Remund, Michael Gibson, Tushar Verma and Manjot Singh for helping me with my extrusion run.

I would like to express my deep gratitude to my co-workers in our group especially Michael Joseph and Lijia Zhu for their support and guidance during my research.

Most importantly, I want to thank my family and friends for their love and encouragement without which nothing could have been possible.

Chapter-1 Introduction

With the increase in population, and also due to changes in the consumer preferences a revolution took place in the food industry to produce different varieties of products with better quality. In the production of different variety food products, along with different other methods, extrusion cooking played an important role especially in the production of expanded products such as breakfast cereal, snack food, pet food etc. Extrusion cooking not only has its impact on the increment of production but also holds great potential in the incorporation of difficult biomaterials such as fiber besides maintaining organoleptic quality of the food product.

1.1 The extrusion process

The extruder is a compilation of different units such as pump for transportation, heat exchanger for heating, bio-reactor shearing and transformation of raw materials into finished extrudates (Chiruvella et al., 1996). Based on the presence of number of screws in the extruder, they can be classified into two types: (i) single screw extruder and (ii) twin screw extruders. The single screw extruder has a simpler geometry as compared to twin screw extruder. However, the twin screw extruders are more versatile in their usage as compared to single screw because of their complex geometry. Based on the type of relative screw rotation direction, the twin screw extruders can be further classified as co-rotating (both screws rotate in the same direction) or counter-rotating (both screws rotate in the opposite directions). According to the interaction of the two screws, there are two types of twin screw extruders: intermeshing (partially, fully) and non-intermeshing (separated, tangential). For intermeshing twin-screw extruders, the separation between the screw axes is less than the outer screw diameter.

The screws rotate inside barrels that are temperature controlled, and it is possible to adjust the number of barrels depending on the desired length of the extruder. The flour, water, and other ingredients are mixed and cooked as they are transported along the barrels by the screws, before passing through the die. The high temperature and high pressure condition inside the extruder results in several phase transitions such as vapor expansion, starch gelatinization, melting, and defragmentation. Along with these phase transitions the other changes such as protein denaturation, amylose-lipid complex formations also take place (Lai and Kokini, 1991). Based on the starch gelatinization taking place inside the cooking zone, the extruded products are classified into cooked (in case of snacks, ready-to-eat foods); and partially cooked (in case of pasta, 3G snacks etc.) products. It is well known fact that, the physical and sensory properties of a food product are largely dependent on the processing conditions of the ingredients used. To survive in the competitive food market, the food industries need to innovate new products. Generally trial and error methods are used for trying out different processing conditions to find the best products that suits the consumer needs. Full scale experimental studies are cumbersome, time consuming, and expensive. In this context, mathematical tools such as modeling or computer simulations play an important role in designing the process tools for the development better product.

1.2 Objectives

The objective of the thesis is to develop a mathematical model capable of predicting the expansion of the extrudates based on the operating conditions such as moisture content, screw speed etc. and study the effect of variability of these parameters on the end product. The main objectives of this study were to

1. Develop and validate a deterministic mathematical model for the behavior of flow inside the extruder to simulate pressure, temperature and energy profiles inside the extruder.
2. Develop and validate a deterministic mathematical model for the expansion and shrinkage of bubbles after the extrudate exits from the die and couple it with model from objective 1 to simulate dynamics of cell structure
3. Develop and validate a stochastic model to study the effect of variability of operating conditions (screw speed, water injection) and material properties (consistency coefficient) on the variability of the end product characteristics.

1.3 References

Chiruvella, R.V., Jaluria, Y. & Karwe, M.V. (1996). Numerical simulation of the extrusion process for food materials in a single screw extruder. Journal of food engineering, 30(3), 449-467.

Lai, L.S., & Kokini, J.L. (1991). Physicochemical changes and rheological properties of starch during extrusion (a review). Biotechnology progress, 7(3), 251-266.

Chapter 2 - Mathematical Modeling of Flow Behavior and Cell Structure Formation During Extrusion

2.1 Introduction

With the increase in population, and also due to changes in the consumer preferences a revolution took place in the food industry to produce different varieties of products with better quality. In the production of different variety food products, along with different other methods, extrusion cooking played an important role especially in the production of expanded products such as breakfast cereal, snack food, pet food etc. Extrusion cooking not only has its impact on the increment of production but also holds great potential in the incorporation of difficult biomaterials such as fiber besides maintaining organoleptic quality of the food product.

The extruder is a compilation of different units such as pump for transportation, heat exchanger for heating, bio-reactor shearing and transformation of raw materials into finished extrudates (Chiruvella et al., 1996). Based on the presence of number of screws in the extruder, they can be classified into two types: (i) single screw extruder and (ii) twin screw extruders. The single screw extruder has a simpler geometry as compared to twin screw extruder. However, the twin screw extruders are more versatile in their usage as compared to single screw because of their complex geometry. Based on the type of relative screw rotation direction, the twin screw extruders can be further classified as co-rotating (both screws rotate in the same direction) or counter-rotating (both screws rotate in the opposite directions). According to the interaction of the two screws, there are two types of twin screw extruders: intermeshing (partially, fully) and non-intermeshing (separated, tangential). For intermeshing twin-screw extruders, the separation between the screw axes is less than the outer screw diameter.

The screws rotate inside barrels that are temperature controlled, and it is possible to adjust the number of barrels depending on the desired length of the extruder. The flour, water, and other ingredients are mixed and cooked as they are transported along the barrels by the screws, before passing through the die. The high temperature and high pressure condition inside the extruder results in several phase transitions such as vapor expansion, starch gelatinization, melting, and defragmentation. Along with these phase transitions the other changes such as protein denaturation, amylose-lipid complex formations also take place (Lai and Kokini, 1991). Based on the starch gelatinization taking place inside the cooking zone, the extruded products are classified into cooked (in case of snacks, ready-to-eat foods); and partially cooked (in case of pasta, 3G snacks etc.) products. It is well known fact that, the physical and sensory properties of a food product are largely dependent on the processing conditions of the ingredients used. To survive in the competitive food market, the food industries need to innovate new products. Generally trial and error methods are used for trying out different processing conditions to find the best products that suits the consumer needs. Full scale experimental studies are cumbersome, time consuming, and expensive. In this context, mathematical tools such as modeling or computer simulations play an important role in designing the process tools for the development better product.

2.2 Literature review

2.2.1 Mathematical modeling

Mathematical modeling acts as an effective tool in understanding the fundamental concepts of the process and also aids in simulating the outcome of a process without actually performing the experiment (Vergnes et al., 2006). Using the mathematical model for extrusion process the physical characteristics of the extruded product such as expansion ratio, bubble radius, open cell

fraction etc. could be predicted using the independent variables (input parameters) such as feed rate, screw speed, water and steam input in the extruder and pre-conditioner etc. The results could be modeled utilizing the mechanistic equations of heat and mass transfer taking place during the process. The concept of modeling the extrusion process started in the beginning of 1940's with the characterization of flow of polymers. The understanding of the behavior of plastics and other polymers is comparatively easier, because of the homogeneity in structure and well characterized physical and rheological properties (Tadmor and Klein, 1978; Tadmor and Gogos, 1979; Karwe and Jaluria, 1990; Gopalakrishna et al., 1992). Thus the polymers possess a predictable behavior upon carrying out mechanical interactions and thermo-mechanical processing. The changes upon interactions between bio-molecules and extruder are very complex (Chiruvella et al., 1996).

2.2.2 Early studies of flow mechanisms

The basic understanding of the flow mechanisms of counter-rotating twin screw extruders first appeared in patents which have shown the forward pumping of filled C-chambers (Wiegand, 1879; Montelius, 1929 and 1936). A clear mathematical discussion of the flow mechanism was first presented by Montelius (1929). The volumetric displacement by a single revolution of screw is given as:

$$V = S\ (\mathrm{A}_S - \mathrm{A}_1 - \ \mathrm{A}_2) \qquad (2\text{-}1)$$

where, A_S is the S-shaped bore volume of the screw casing, A_1 is the cross-sectional area of the single thread screw A and A_2 is the cross-sectional area of the double thread screw. All of these cross-sections are taken as right angles to the axis, and *S* represents the pitch of screw.

The modified expression for forward pumping capacity is given by Kiesskalt (1927) is given as:

$$Q = m\mathrm{V}_c - \mathrm{Q}_{leak} \tag{2-2}$$

where, *m* is the number of thread starts, V_c shows the total C-chamber volume and Q_{leak} is a backward leakage flow.

A closed C-shaped chamber was produced by the intermeshing of two screws with left-handed and right-handed flights is advanced by the rotation of the screws towards the die (Rauwendaal, 1986). The extrusion rate through an intermeshing counter-rotating twin screw extruder is given as:

$$Q = 2mN\mathrm{V}_c \tag{2-3}$$

where, *Q* is the volumetric throughput, *m* is the number of the screw thread starts, *N* is the screw speed and *Vc* is the associated the C-chamber volume per screw. Most of these flow mechanism equations were developed considering the polymer extrusion. The researchers in 1960's started looking at determining the chamber volume *Vc* as:

$$\mathrm{V}_c = \frac{\mathrm{V}_b - \mathrm{V}_{sr} - m\mathrm{V}_f - m\mathrm{V}_{cal}}{m} \tag{2-4}$$

where, V_b is the volume of a barrel half over one pitch. V_{sr} is the volume of the screw root, V_f is the-volume of the screw flight, V_{cal} is the volume of the intermeshing region,

$$\mathrm{V}_b = \pi r^2 S \tag{2-5}$$

$$\mathrm{V}_b = m(R-H)^2 S \tag{2-6}$$

$$\mathrm{V}_f = \int_{R-H}^{R} b(r) 2\pi r dr \tag{2-7}$$

where, R is screw radius, H is channel depth, S is the pitch, *b(r)* is the width of the screw flight at position r.

2.2.3 Viscosity models

The main viscosity models found in literature are summarized in Table 2.1. To relate the viscosity of the product with the shear rate, many rheological models such as; power-law, Cross law, Carreau law exist. The apparent viscosity (μ) of a product is measured with:

$$\mu = \frac{\sigma_w}{\gamma_w} \tag{2-8}$$

where, σ_w is the shear stress at the wall (and expressed as a function of pressure drop), while γ_w is the wall shear rate and depends on the flow rate.

It was shown that, the maize and wheat flour can be modelled as power-law fluids $\mu = K\gamma^{n-1}$, with a flow behavior index, *n*, within the range 0.2 to 0.6 (Guy and Horne, 1988 and Lai and Kokini, 1991). The influence of operating conditions on the consistency *K* and the power-law index *n* of the cereal were first studied by Vergnes *et al.* (1993). The conclusions drawn from their study are as follows:

- an increase in moisture content from 20.5 to 27.1% leads to an increase in *n* from 0.35 to 0.46, and a decrease in *K* from 9500 to 2750 Pa s^n (at *T*=165 to 170 °C);
- an increase in melt temperature from 167 to 192 °C, with a moisture content of 27.1%, leads to a decrease in *K* from 2650 to 2010 Pa s^n, and has nearly no influence on *n* (varying between 0.52 and 0.50).

Kirby et al. (1988) and Guy and Horne, (1988) showed that, an increase in temperature results in a decrease in viscosity. The decrease in viscosity is generally expressed in terms of an Arrhenius type relation with an activation energy depending on the extrusion conditions (summarized in Table 1). It was also shown that, the viscosity follows an exponential relationship with respect to moisture content X: $\mu = k_0 \exp(kX)$; (k<0). It was also found that different rheological

properties are obtained if the branched polymers are stretched or in tension (Padmanabhan, 1995Viscous dissipation cannot be neglected especially if the diameter of the die is very less and the viscosity of the food product is very high. In this study, viscous heating was assumed to be negligible due to bigger diameter of the die.

Table 2-1 Viscosity models discussed in literature

Model Name	**Apparent Viscosity**	**Note**	**References**
Power law	$\mu = K\dot{\gamma}^{n-1}$		
Power law modified	$\mu = K\dot{\gamma}^{n-1} \exp (K_1 / T) \exp (K_2 X)$	Moisture content (X) and temperature (T)	Alvarez-Martinez et al., 1988; Kokini et al., 1991;and Fan et al., 1994
Modified Harper's equation	$\mu = K\dot{\gamma}^{n-1} \exp ([\Delta H + K_1 X] / RT) \exp (- [K_{20} + K_{21} T] X) DG^{K1}$	Degree of gelatinization (DG) Moisture Content (X)	Kokini et al., 1991
Study by Bloksma and Nieman	$\mu = K\dot{\gamma}^{n-1} \exp ([- \Delta H / R] ([1/T] – [1/T_0])$	Temperature	Bloksma and Nieman, 1975
Power law with K and n affected by X and T	$\mu = K\dot{\gamma}^{n-1}$ $K = K_0 \exp \{ (E/R) ([1/T] – [1/T_0]) – \beta (X – X_0) \}$ $n = \alpha_1 T + \alpha_2 X + \alpha_3 T . X$	Moisture Content X, X_0 and temperature T and T_0	Della Valle et al., 1993

Study by Senouci and Smith	$\mu = K\dot{\gamma}^{n-1} \exp(\Delta H / RT) \exp(kX) N^{-a}$	N is the screw speed^0	Senouci and Smith, 1988
Study by Bouzaza et al.	$\mu = K\dot{\gamma}^{n-1} (1 - k_1 W) \exp(k_2 X)$	W is the specific Mechanical Energy^0	Bouzaza et al., 1996

2.2.4 Microscopic modeling of bubble formation

The modeling of bubble growth surrounded by a fluid under a given pressure has started many years ago. A large number of studies were made, with different degrees of complication. Barlow and Langlois (1962), with their model on bubble growth in a Newtonian liquid, are probably pioneers in the domain of bubble growth modeling. A simple model describing inertia-controlled and heat-diffusion-controlled growth in a uniformly superheated liquid and in a non-uniform temperature field was developed by Mikic et al. (1970). Yang and Yeh (1966) further advanced and derived equations for a bubble growing in a power-law fluid, a Bingham fluid, and a Newtonian fluid. Street et al. (1968) further advanced and proposed models for viscoelastic fluid and power-law fluid. The concept of cell model was first introduced by Amon and Denson (1984). In their study, they considered that finite number of molecules for the bubble growth are available, since the bubble is surrounded by an envelope of liquid (with a finite thickness) which was opposed to other studies where the radius increases with time without any limitation. Venerus et al. (1997, 1998, and 2001) conducted studies, where they studied the range of applicability of such a model with the assumption of a thin boundary layer.

The researchers further advanced and developed models for simultaneous bubbles, where they studied each bubble individually (Arefmanesh et al., 1990). In another study, they also developed a method for obtaining the concentration profile in the envelope surrounding the bubble without making the assumption of a second- or third-order polynomial (Arefmanesh et al., 1992). More recently, Ramesh and Malvitz (1998, 1999) considered surface evaporation or gas loss condition in their model not only to molding process, but also to extrusion process. Shafi and co-workers predicted polymer foam processes using the models of bubble growth in addition with nucleation models (1996, 1997 and 1998). A simple analytical expression for bubble growth as a function of time in a power-law fluid was developed by Huang and Kokini (1999). Pai and Favelukis (2002) focused their study on the domain of validity of the assumption of isothermal bubble growth. Most of the studies discussed above were done for polymers, Shimiya and Yano (1987) were the first people focused on wheat flour. Fan et al. (1994, 1999) and Mitchell et al. (1998) developed models applied to extrudate expansion or to oven rise of dough during baking, while other researchers adapted the methods from polymer industry to agro-business industry (Huang and Kokini, 1999; Schwartzberg et al., 1995; Shah et al., 1998; Achanta et al., 1999). With the advancement of technology and availability of modeling software, attempts are made to couple these microscopic models (at the bubble scale) with models for the macroscopic scale. For example, Shimoda et al. (2001) combined classical nucleation rate and bubble growth models with a power-law fluid model. They studied the bubble growth in the die region only and the simulation results showed good agreements with experiments: when the inlet pressure increases, the onset position of foaming moves toward the die exit. But they have not studied the flow out of the die, and they have assumed a 4^{th} order profile of concentration in blowing agent in the envelope. Alavi et al. (2003a, 2003b) coupled a microscopic model for bubble growth with

macroscopic exchanges of mass and heat. This model is applied for extrusion at low temperature with supercritical CO_2.

2.3 Model Development and Validation

2.3.1 Assumptions of the model

Modeling of food extrusion process is a complex process because of the heterogenous properties of the food materials and their phase transitions are not well-defined. Hence there were several assumptions considered in the model.

1) The temperature increase inside the extruder only takes place due to conveying of melt inside the extruder. The effect of thermal energy of the barrel on the temperature evolution inside the extruder is considered as negligible.
2) The flow is steady, isothermal and fully developed and the net flow in axial direction is only considered. The material flowing inside the extruder is considered to be homogenous and incompressible fluid following power law.
3) Gravity effect is negligible and is ignored.
4) The change of raw material from granular state to melt fluid inside the extruder is assumed to be transformed suddenly. This change is assumed to take place as soon as barrel becomes full.
5) Leakage flow is ignored.
6) The moisture content is always expressed in dry basis (unless explicitly mentioned) i.e. mass of water per unit mass of dry solids.

7) Expansion due to die swell is neglected and expansion considered is only due to evaporation of water. Expansion due to die swell is significant at lower temperatures (Fan et al., 1994).
8) The diffusion coefficient and viscosity coefficient is considered to be a function of moisture content and temperature.
9) The process dynamics at the microscopic level is studied by considering all bubbles to be uniform and spherical in shape.
10) The phenomenon of coalescence is neglected.
11) Sectional expansion ratio is considered to be the expansion ratio and axial expansion of the extrudate is not considered.
12) The complex chemical reactions and degradation of starch components are neglected due to difficulty in modeling such reactions.

2.3.2 Modeling the flow behavior inside the extruder

Tayeb et al. (1989) and Yacu (1985) developed a basic model for a twin screw extruder and hence they are used as to develop the basic model inside the extruder. Tayeb et al. was Pressure profile is developed based on Tayeb et al. (1989) and temperature profile is developed based on Yacu (1985). They do not consider the effect of thickness of the screw flight. Hence, the equations are modified to incorporate the screw thickness effect as well based on Rossen and Miller (1973). It is assumed that the material becomes fluid melt as soon as the barrel is full. There are two sections inside the extruder: Solid conveying section and melt pumping section. The actual length of the melt pumping section is the parameter which is affected by screw profile, screw speed, throughput, viscosity of the material and the overall flow resistance (Yacu, 1985). The temperature increases very quickly in the melt pumping section. Viscosity of the

material is based on temperature and moisture content and hence it changes as well. Hence, the actual length of the melt is assumed. The temperature and pressure profiles are developed along the barrel and final temperature and pressure at the end of the barrel are obtained.

The pressure drop across the die is calculated based on the final temperature obtained at the end of the barrel. If the pressure drop across the die is greater than the pressure at the end of the barrel, the actual length of the melt is increased. If the pressure drop across the die is lesser than the pressure at the end of the barrel; the actual length of the melt is decreased and the same pressure and temperature profiles are developed. This evaluation is done till the pressure drop is almost same as the final pressure at the end of the barrel.

2.3.2.1 Temperature profile

The viscous heat dissipation is negligible as the screws in this section are only partially full. As we are assuming that the effect of thermal energy of the barrel on the temperature evolution inside the extruder is considered as negligible, the temperature does not increase in the conveying section. Yacu (1985) is used as a basic to develop the temperature profile inside the extruder.

The screw sections become full in the melt pumping section and the raw material becomes melt. The temperature profile along the barrel is developed based on the mechanical energy generated. The amount of energy generated (ΔE) from an element of thickness Δx of screw (Yacu, 1985) is

$$\Delta E = \frac{4\mu N^2 \Delta x(\pi D - \sqrt{2Dh})}{h} \tag{2-9}$$

where μ is viscosity of the melt given by equation 2-10, N is screw speed, D is the diameter of the screw and h is screw channel depth.

$$\mu = K\gamma^{n-1} \quad (2\text{-}10)$$

where $$K = 4.224 * \exp\left(\frac{2650}{T} - 25\ \frac{X_w}{1+X_w}\right) \quad (2\text{-}11)$$

$$\gamma = \frac{\pi DN}{h} \quad (2\text{-}12)$$

where K is consistency coefficient of the melt given by equation 2-11 at temperature T and moisture content X_w; n is flow behavior index.

The increase in temperature (ΔT_E) inside the extruder due to the energy generated (ΔE) (Yacu, 1985) is given by

$$\Delta T_E = \frac{\Delta E}{(m_f C_p)} \quad (2\text{-}13)$$

where m_f is mass flow rate of the product exiting the die and C_p is specific heat at moisture content X_w given in equation 2-14

$$C_p = 1.5 + (4.2 * X_w) \quad (2\text{-}14)$$

Specific mechanical energy (SME) during the extrusion is calculated by

$$SME = \frac{\sum \Delta E}{m_f} \quad (2\text{-}15)$$

2.3.2.2 Pressure profile

No pressure is developed in the solid conveying section as the screws are only partially full. Hence, the entire pressure is generated in the melt pumping section. Tayeb et al. (1989) is used as a basic to develop the pressure profile inside the extruder.

The pressure developed is calculated using the flow rate equation. As we are assuming that there is no leakage flow; the flow rate consists of two components: Drag flow along the direction of flow and pressure flow acting in opposite direction to the direction of flow due to the generation of pressure.

$$\frac{Q_v}{lv} = -F_P \frac{1}{32\mu}\frac{\Delta P_E}{\Delta\Theta}(D^2 - D_i^2)[1 - \left(\frac{2DD_i}{D^2 - D_i^2}\ln\left(\frac{D}{D_i}\right)\right)^2]\left(1 - \frac{n_f e}{t}\right)$$

$$+ F_D \frac{1}{4}\pi N D^2 cos\Phi[1 - (\frac{D_i^2}{D^2 - D_i^2}\ln\left(\frac{D}{D_i}\right)^2)]\left(1 - \frac{n_f e}{t}\right) \quad (2\text{-}16)$$

where Q_v is the volumetric flow rate and lv is the channel width. The term $\left(1 - \frac{n_f e}{t}\right)$ is incorporated to include the effect of screw thickness based on Rossen and Miller (1973). The equation 2-16 helps in calculating the pressure gradient $\frac{\Delta P_E}{\Delta\Theta}$ where $\Delta\Theta = \frac{\Delta x}{\pi D}$. This helps us in calculating the increase in pressure from an element of thickness Δx of screw.

F_D and F_P are the correcting shape factors for drag flow and pressure flow respectively and are dependent on depth/width ratio of the channel (Rauwendaal, 1986). The value of these parameters is obtained from Jiang, 2008.

$$F_D = 1 - (0.5356 * n^{-0.4})\frac{h}{lv} \quad (2\text{-}17)$$

$$F_P = 1 - (0.6216 * n^{-0.4})\frac{h}{lv} \quad (2\text{-}18)$$

2.3.2.3 Pressure drop across the die

The pressure drop across the die P_f is given by the fluid flow equation for laminar flows in non-Newtonian fluids (Steffe, 1992).

$$\frac{dP_f}{dx} = -\frac{4K}{[d(x)]^{3n+1}}(\frac{8m_f}{\pi\rho})^n(\frac{3n+1}{n})^n \quad (2\text{-}19)$$

Where

$$d(x) = d_{en} - \left(\frac{d_{en} - d_{ex}}{L_d - L_{d1}}\right)x \quad \text{for } x \geq L_d - L_{d1} \quad (2\text{-}20)$$

$$d(x) = d_{ex} \quad \text{for } x \leq L_d - L_{d1} \quad (2\text{-}21)$$

The d_{en} represents the diameter of the entrance of the die and d_{ex} represents the die diameter at the exit. L_d and L_{d1} are the die dimensions as specified in the Figure 2-1.

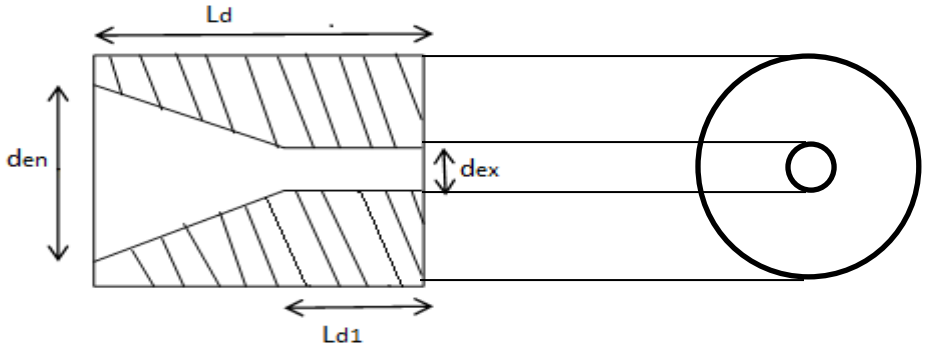

Figure 2-1 Dimensions of the die

2.3.3 Microscopic model

The microscopic model comprises bubble growth in the melt. The bubble growth takes place due to the pressure difference between saturation vapor pressure and opposing pressure components which include elastic stress, yield stress, tensile stress and atmospheric pressure. As the bubble grows due to conversion of moisture to steam, more moisture moves inside the microscopic shells from the matrix. The process dynamics at the microscopic level is studied by considering all bubbles to be uniform and spherical in shape. Schwartzberg et al. (1995) developed a model for vapor induced puffing (VIP) in popcorn kernels and is used a base to develop microscopic model.

2.3.3.1 Bubble expansion and shrinkage

The domain is considered to be finite. It consists of a single bubble filled with vapor and surrounded by material. The bubble is considered to be spherical in shape and it is divided into N_{mi} shells for finite element modeling (Figure 2-2). Radius of the bubble is R and the cell wall thickness of the domain is W and radius of the domain is L; which is R+W. Initial values of these parameters are indicated with subscript o.

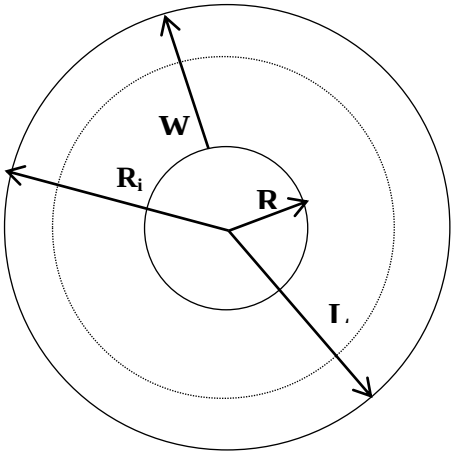

Figure 2-2 Microscopic shells of the bubble

Bubble expansion and shrinkage takes place depending on the pressure components acting on the wall of an individual bubble. These pressure components include vapor pressure (P_w), elastic stress (P_e), tensile stress ($\frac{2\sigma}{R}$), yield stress (P_y) and atmospheric pressure (P_a) (Figure 2-3).

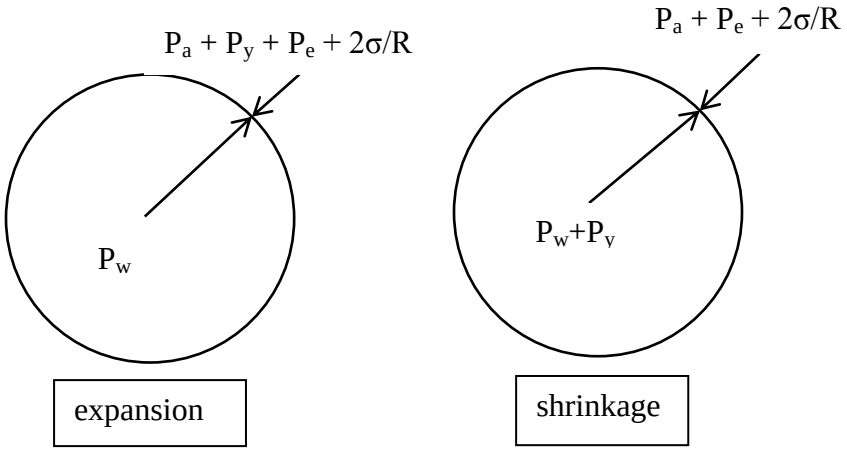

Figure 2-3 Pressure components acting on individual bubble during expansion and shrinkage

If the resultant pressure of these pressure components acts in the outward direction, it leads to expansion of bubble. Therefore the rate of expansion is dependent on $P_w - P_a - P_e - P_y - \frac{2\sigma}{R}$ and the rheological properties of the domain. As the water keeps diffusing into the bubble and temperature falls, the vapor pressure decreases with time. Hence, if the resultant pressure acts in the inward direction, the bubble shrinks and the rate of shrinkage is dependent on $P_a + P_e + \frac{2\sigma}{R} - P_w - P_y$.

Vapor pressure (P_w) of the moisture content in the bubble is given by equation 2-22. (Schwartzberg et al., 1995)

$$P_w = P_{wsat} a_w \tag{2-22}$$

where P_{wsat} is the saturation vapor pressure at a given absolute temperature (T) of the bubble and a_w is the water activity at the surface of the cell. X_{wc} in equation 2-24 represents the moisture content at the inner most layer of the bubble. (Schwartzberg et al., 1995)

$$P_{wsat} = 1002.2 \times \exp\left[9.43699 - \frac{3867.44}{T - 43.37}\right] kPa \tag{2-23}$$

$$a_w = BX_{wc} + \frac{CX_{wc}}{F + X_{wc}} \tag{2-24}$$

Where

$$B = -0.5362 - 0.001394 \times T + \frac{2.0474 \times (468.9 - T)}{477.42 - T} \tag{2-25}$$

$$C = 0.2479 + 0.001216 \times T \tag{2-26}$$

$$F = 0.002004 + 0.3165 \times 10^{-5} T \tag{2-27}$$

Elastic stress (P_e) acting on the cell wall is given by equation 2-28. (Schwartzberg et al., 1995)

$$P_e = E\left[\frac{5}{2} - \frac{2R_o}{R} - \frac{1}{2}\left(\frac{R_o}{R}\right)^4\right]\left(\frac{L^3 - R^3}{L^3 + 2R^3}\right) \tag{2-28}$$

Where

$$E = E_b \ (X_a \geq 0.14) \tag{2-29}$$

$$E = E_b \exp\left[\beta_f(0.14 - X_a)\right] \ (X_a < 0.14) \tag{2-30}$$

$$E_b = E_r \exp[0.1(T_{ref} - T)] \tag{2-31}$$

E_r = 5 kPa, β_f = 73, T_{ref} = 383

Here X_a means the average moisture content for all layers.

Yield stress (P_y) acting on the cell wall is given by equation 2-32. (Schwartzberg et al., 1995)

$$P_y = 3.464\tau_o \ [1/3 + ln(L/R) \ ] \tag{2-32}$$

Where

$$\tau_o = \tau_b \ (X_a \geq 0.14) \tag{2-33}$$

$$\tau_o = \tau_b \exp\left[\beta_f(0.14 - X_a)\right] (X_a < 0.14)$$

$$\tau_b = \ \tau_r \exp[0.1(T_{ref} - T)] \tag{2-34}$$

τ_r = 4.65 kPa, β_f = 73, T_{ref} = 383 K

Neglecting the inertial effects, the equation 2-35 is used to evaluate the rate of change of bubble radius (ΔR) in timestep Δt during expansion based on different pressure components obtained above. (Schwartzberg et al., 1995)

$$\Delta R = R(\Delta t)\left[\frac{P_w - P_a - P_y - P_e - \frac{2\sigma}{R}}{\frac{4(2/\sqrt{3})^{n-1}}{n}[\xi + K_c - K_s(\frac{R}{L})^{3n}]}\right]^{1/n} \tag{2-35}$$

Where

$$\xi = \sum_{i=1}^{N_{mi}+1} [K_i - K_{i-1}](\frac{2R}{R_i + R_{i-1}})^{3n} \tag{2-36}$$

ξ in equation 2-36 accounts for the changes in consistency index (K) across the domain due to differences in moisture content across the different layers of the bubble and subscript i refers to the i^{th} shell in the discretization of the spherical bubble. The consistency index (K) at a given temperature T and moisture content X_w is given in equation 2-11.

If the resultant pressure on the cell wall acts in the inward direction, the bubble shrinks and the rate of change of bubble radius is given by equation 2-37. (Schwartzberg et al., 1995)

$$\Delta R = R(\Delta t)[\frac{P_a + P_e + \frac{2\sigma}{R} - P_w - P_y}{\frac{4(2/\sqrt{3})^{n-1}}{n}[\xi + K_c - K_s(\frac{R}{L})^{3n}]}]^{1/n} \quad (2\text{-}37)$$

The radius of the shells R_i and the domain radius (L) is obtained using the equations 2-38 and 2-39 respectively. (Schwartzberg et al., 1995)

$$R_i^3 = [R^3 + \frac{3}{4\pi}(\frac{\Delta M}{2\rho_m} + \sum_{j=1}^{i-1}\frac{\Delta M}{\rho_j})]^{1/3} \quad (2\text{-}38)$$

$$L = [R^3 + \frac{3}{4\pi}\sum_{i=1}^{N_{mi}}\frac{\Delta M}{\rho_i}]^{1/3} \quad (2\text{-}39)$$

ΔM in the above equations represents the mass of dry solid in each layer of the bubble ($\Delta M = \frac{M}{N_{mi}}$) and ρ_i is the density of the dry matter in i^{th} shell of the individual bubble. ρ_m in equation 2-38 is the average density of the half of the i^{th} shell completing the spherical volume of radius and is given as $0.75\ \rho_i + 0.25\ \rho_{i-1}$.

Mass of dry solid in domain M is calculated by using $M = \frac{\rho_{dry}}{N_{bubble}}$ where ρ_{dry} is the density of dry unexpanded melt and N_{bubble} is the number of bubbles/m^3 of unexpanded material.

2.3.3.2 Diffusion of water

During the expansion of the bubble, water vapor diffuses into the bubble from the domain. Part of the moisture present in the spherical shells of the bubble is slowly converted into steam which is trapped inside the inner most layer of the bubble. As more and more moisture is converted to steam from the inner-most layer of the bubble, diffusion takes place in the spherical shells of the bubble in the inward direction. X_i represents the moisture content of the i^{th} spherical shell at any

instant of time and the change in moisture content ΔX_i in timestep Δt is calculated using the equation 2-40. (Schwartzberg et al., 1995)

$$\Delta X_i = \frac{\Delta t}{\Delta M}\left[\frac{D_{i+1/2}A_i(\rho_{i+1}X_{i+1} - \rho_i X_i)}{(R_{i+1} - R_i)} - \frac{D_{i-1/2}A_{i-1}(\rho_i X_i - \rho_{i-1}X_{i-1})}{(R_i - R_{i-1})}\right] \quad (2\text{-}40)$$

where $$D_{i+1/2} = \frac{D_i + D_{i+1}}{2} \text{ and } D_{i-1/2} = (D_i + D_{i-1})/2 \quad (2\text{-}41)$$

Equation 2-32 is used to calculate the change in all X_i except X_1, X_N, X_C and X_S. It is assumed that diffusion coefficient is a function of moisture content and temperature. Here D_{i-1}, D_i and D_{i+1} are calculated at X_{i-1} , X_i and X_{i+1} respectively and temperature T. Diffusivity of water at given temperature T and moisture content X_w is calculated using equation 2-42 (Van der Lijn, 1976).

$$D_w = 1.35 \times 10^{-8} \exp\left[\frac{-21.61(548 - T)(1.194 + 3.68X_w)}{T(1 + 18.98X_w)}\right] m^2/s \quad (2\text{-}42)$$

$$A_i = (4\pi)\left[R^3 + \frac{3}{4\pi}\sum_{j=1}^{i}\frac{\Delta M_j}{\rho_j}\right]^{2/3} \quad (2\text{-}43)$$

A_i gives the area for diffusion for i_{th} layer which is calculated using equation 2-43.

ΔX_N and ΔX_S are calculated using equations 2-44 and 2-45 respectively. (Alavi et al., 2003)

$$\Delta X_N = \frac{\Delta t}{\Delta M}\left[A_{N-1}D_{N-1/2}\frac{(\rho_{N-1}X_{N-1} - \rho_N X_N)}{(R_N - R_{N-1})} - A_S D_S \frac{(\rho_N X_N - \rho_S X_S)}{(L - R_N)}\right] \quad (2\text{-}44)$$

$$\Delta X_S = \frac{2D_S(\Delta t)(X_N - X_S)}{(L - R_N)^2} \quad (2\text{-}45)$$

Here D_S is diffusivity at domain surface and $A_S = 4\pi L^2$ is the surface area of the domain.

Change in mass of water vapor in the bubble during timestep Δt is given by equation 2-46. (Schwartzberg et al., 1995)

$$\Delta Q = \frac{4\pi R^2}{3v}[3(\Delta R) - \alpha(\Delta T) + \zeta(\Delta X_c)] \quad (2\text{-}46)$$

where

$$\alpha = \frac{GR}{P\upsilon}\left[1 - T\frac{d(lnP_{wsat})}{dT} - \frac{T}{a_w}\frac{\partial a_w}{\partial T}\right] \quad (2\text{-}47)$$

$$\zeta = \frac{GRT}{P\upsilon a_w}\frac{\partial a_w}{\partial X_{wc}} \quad (2\text{-}48)$$

$$G = 0.4561\ \frac{m^3 kPa}{kg.K} \quad (2\text{-}49)$$

Here υ is the specific volume of water vapor given in equation 2-50

$$\upsilon = \frac{GT}{P_w} - 0.01637\ \frac{m^2}{s} \quad (2\text{-}50)$$

Change in moisture content at the innermost surface of the pore ΔX_C is calculated using equation 2-51. (Schwartzberg et al., 1995)

$$\kappa \Delta X_c = \frac{D_c(X_1 - X_C)\Delta t}{(R_1 - R)(\Delta r)} + \alpha(\Delta T)\theta - 3(\Delta R)\theta \quad (2\text{-}51)$$

where

$$\kappa = 1 + \zeta\theta,\ \theta = \frac{1}{3\nu\rho_c}\left[\frac{1}{\Delta r} - \frac{2}{R}\right] \quad (2\text{-}52)$$

$\Delta r = \frac{R}{3}$ when $(R_1\text{-}R) > R$ and $\Delta r = R_1 - R$ when $(R_1\text{-}R) < R$ (2-53)

Here ρ_c is the density at innermost surface of the pore.

ΔX_1 is calculated using the equation 2-54. (Schwartzberg et al., 1995)

$$\Delta X_1 = \frac{1}{M}\left[\frac{D_{3/2}A_1(\rho_2 X_2 - \rho_1 X_1)\Delta t}{(R_2 - R_1)} - \Delta Q\right] \quad (2\text{-}54)$$

There are instabilities in the model if the timestep (Δt) used is not small enough. The value of the timestep used is given in equation 2-55.

$$\Delta t = 0.01 * \frac{(L - r_N)^2}{2D_s} \quad (2\text{-}55)$$

The value of the timestep is dependent on the cell wall thickness. As the cell wall thickness is very low after the expansion of the bubble, the value of timestep (Δt) used during shrinkage is given in equation 2-56

$$\Delta t = \frac{(L - r_N)^2}{2D_s} \tag{2-56}$$

2.3.3.3. Open cell fraction and open pore volume

During the expansion of the bubble, the tensile stress S_w develops in the pore walls. If the tensile stress S_w developed in a cell exceeds the tensile failure stress S_f; the cell wall ruptures and an open cell is formed. Coalescence of adjacent cells can take place when the cells rupture and the radius of individual cell can increase. As the phenomenon of coalescence is neglected in this model, the open cells lose their ability to expand further. In reality, the initial radii and other properties vary for all the bubbles. Therefore, all bubbles do not rupture simultaneously and the expansion of the bubbles and the extrudate continues. The value of fraction of number of open cells f_o varies between 0 to 1. A modified normal distribution of S_w and S_f is attempted to describe the variation of f_o. The change in open cell fraction Δf_o in timestep Δt is given by equation 2-57. (Schwartzberg et al., 1995)

$$\Delta f_o = \frac{\Delta Z}{\sqrt{2\pi}} \exp[\frac{-Z^2}{\psi}] \tag{2-57}$$

where

$$Z = \frac{(S_w - S_f)}{2S_f} \tag{2-58}$$

Here ψ determines the spread of f_o. In this model, ψ is considered as 2.5. At the beginning of expansion S_w is given by equation 2-59 and towards the end of expansion when W<<R, S_w is given by equation (2-60).

$$S_w = \frac{\Delta P_w R^2}{W^2 + 2RW} \tag{2-59}$$

$$S_w = \Delta P_w R/2W \tag{2-60}$$

The failure stress S_f is given by equations 2-61 and 2-62.

$$S_f = S_r \ (X_a \geq 0.14) \tag{2-61}$$

$$S_f = S_r \exp[\beta_s(0.14 - X_a)] \ (X_a < 0.14) \tag{2-62}$$

$$S_r = S_m \exp[0.1(T_{ref} - T)] \tag{2-63}$$

S_m = 4000 kPa, β_s = 73, T_{ref} = 383 K

Fraction of open pore volume F_o after timestep k is given by equation 2-64.

$$F_o = \frac{\sum_{j=1}^{k} (\Delta f)_{o_j} {R_j}^3}{(1 - f_o)_k {R_k}^3 + \sum_{j=1}^{k} (\Delta f_o)_j {R_j}^3} \tag{2-64}$$

2.3.4 Macroscopic model

The macroscopic model accounts for the heat and mass transfer that takes place at the extrudate level. The process dynamics at the macroscopic level is studied by considering the extrudate in cylindriacal shape. Alavi et al (2003) is used a base to develop macroscopic model.

2.3.4.1 Heat transfer

For heat transfer at the macroscopic level, the cylindrical extrudate is discretized into finite number of concentric cylindrical shells (N_b) (figure 2-4). The extrudate cools down after it exits the die due to conduction, convection and evaporation. The fall of temperature due to evaporation is discussed later in section 2.7 where the microscopic and macroscopic models are coupled. The heat transfer in the outermost layer takes place due to conduction with the adjacent layer and convection with the atmosphere and heat transfer in the inner layers takes place due to conduction.

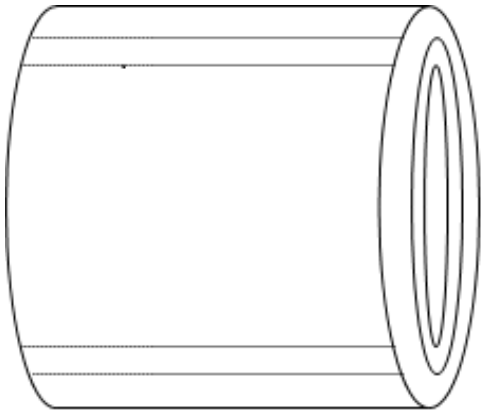

Figure 2-4 Macroscopic shells of the extrudate

The numerical form of unsteady state heat transfer equation is taken from Geankoplis (1993). The local temperature of each shell is denoted by T_j (j = 1 to N_b) and average temperature is obtained by taking the mean of all temperatures. The change in temperature ΔT_j in timestep Δt is calculated using equation 2-65. This equation is applicable for all ΔT_j except ΔT_0 (temperature at center where j=0) and ΔT_{Nb} (layer in contact with atmosphere)

$$\Delta T_j = \frac{1}{M_T}\left(\frac{2j+1}{2j}T_{j+1} - 2T_j + \frac{2j-1}{2j}T_{j-1}\right) \tag{2-65}$$

where

$$M_T = \frac{(\Delta x)^2}{\alpha \Delta t} \tag{2-66}$$

Here Δx is the discretization step size, α is the thermal diffusivity in the starch matrix and Δt is the timestep. The change in temperature at the center where j = 0 is given by equation 2-67

$$\Delta T_0 = \frac{4}{M_T}(T_1 - T_0) \tag{2-67}$$

The temperature change in outermost layer takes place due to thermal conduction with the adjacent layer as well as due to convective transfer with the atmosphere. The temperature at the outer surface of the cylinder where j = N_b is given by equation 2-68

$$T_{N_b} = \frac{N_b N_T}{\frac{2N_b - 1}{2} + N_b N_T} T_a + \frac{(2N_b - 1)/2}{\frac{2N_b - 1}{2} + N_b N_T} T_{N_b - 1} \quad (2\text{-}68)$$

Where

$$N_T = \frac{h\Delta x}{k_{eff}} \quad (2\text{-}69)$$

$$k_{eff} = k_{solid}[1 + \frac{3\epsilon(1 - \frac{k_{solid}}{k_{gas}})}{(1 - \epsilon) + (2 + \epsilon)\frac{k_{solid}}{k_{gas}}}] \quad (2\text{-}70)$$

h in equation 2-69 is the convective heat transfer coefficient and k_{eff} is the effective thermal conductivity of the porous extrudate. The equation for effective thermal conductivity is given by 2-70 and it accounts for the porosity of the extrudate as well as the thermal conductivity in the solid and gas phase (Alavi et al., 2003).

2.3.4.2 Mass transfer

Mass transfer takes place at both microscopic and macroscopic level. As the outermost layer is in contact with atmosphere, water diffuses from the outermost layer into the atmosphere. The numerical form of unsteady state mass transfer equation is taken from Geankoplis (1993). The local mositure of each shell is denoted by C_j (j = 1 to N_b) and average moisture (C_{avg}) is obtained by taking the mean of all temperatures. The change in moisture ΔC_j in timestep Δt is calculated using equation 2-71. This equation is applicable for all ΔC_j except ΔC_0 (moisture at center where j=0) and ΔC_{Nb} (layer in contact with atmosphere)

The effective diffusivity of the moisture content (D_{eff}) is calculated by considering porosity of the extrudate into account (equation 2-73).

$$\Delta C_j = \frac{1}{M_c}(\frac{2j + 1}{2j} C_{j+1} - 2C_j + \frac{2j - 1}{2j} C_{j-1}) \quad (2\text{-}71)$$

where

$$M_c = \frac{(\Delta x)^2}{D_{eff}\Delta t} \tag{2-72}$$

Here Δx is the discretization step size, D_{eff} is the effective diffusivity due to porosity of the extrudate which is calculated using equation 2-73.

$$D_{eff} = \frac{1-\epsilon}{\zeta} \times D_w \tag{2-73}$$

Є and ζ in equation 2-73 represent the porosity and tortuosity of the extrudate respectively and D_w is the diffusivity given by equation 2-42. The change in moisture at the center where j = 0 is given by equation 2-74

$$\Delta C_o = \frac{4}{M_c}(C_1 - C_o) \tag{2-74}$$

At the outer most layer of the extrudate, the moisture diffusion takes place from the inner layers as well as convection takes place from the outermost layer. The moisture at the outer surface of the cylinder where j = N_b is given by equation 2-75.

$$C_{N_b} = \frac{N_b N_c}{\frac{2N_b-1}{2} + N_b N_c} C_a + \frac{(2N_b-1)/2}{\frac{2N_b-1}{2} + N_b N_c} C_{N_b-1} \tag{2-75}$$

where

$$N_c = \frac{K_{xc}\Delta x}{D_{eff}} \tag{2-76}$$

Here C_a is the ambient moisture content and K_{xc} is the mass transfer coefficient of water in the starch matrix.

2.3.5 Micro-Macro Coupling

The linking of microscopic modeling with macroscopic modeling includes the linking of moisture contents of microscopic shells of bubble to macroscopic shells of the extrudate; temperature fall of the extrudate due to evaporation of water and coupling the growth of the bubble with the expansion of the extrudate.

2.3.5.1 Linking of moisture content

In order to link the macroscopic diffusion model to microscopic diffusion, the microscopic moisture content of all the shells X_i is reduced by same extent as reduction in C_{avg} at each timestep.

2.3.5.2 Temperature reduction due to evaporation

ΔQ is the amount of water evaporated from a bubble of mass (M) in a timestep Δt. It is calculated using equation 2-46. This is linked to macroscopic model by decreasing the temperatures across all the macroscopic shells by $\frac{\Delta Q \lambda}{M C_p}$ where λ is the latent heat of vaporization and C_p is the specific heat calculated using equation 2-14.

2.3.5.3 Expansion ratio of the extrudate

As assumed, we are neglecting the axial expansion of the extrudate. Sectional expansion ratio is considered to be the expansion ratio. The expansion of the extrudate is coupled to the growth of the bubble by using a modified form of equation used by Schwartzberg et al. (1995).

Expansion ratio (ER) is calculated using the equation 2-77.

$$ER = [1 - f_o]_k \left(\frac{L_k}{L_o}\right)^3 + \sum_{j=1}^{k} (\Delta f_o)_j \left(\frac{L_j}{L_o}\right)^3 \quad (2\text{-}77)$$

The first term in the equation accounts for expansion due to closed cells whereas the second term accounts for expansion due to open cells.

2.3.6 Algorithm development

The model equations are written in Visual Basic with EXCEL™ as an interface to input the parameters and display the output results such as bubble radius, expansion ratio and open cell fraction versus time. The basic algorithm used in developing the code is shown in Fig 2-5. The

typical simulation time for the code is about 30-45 minutes depending on the computational ability of the computer and the code stops if the number of timesteps is greater than 200000. This number is chosen based on computational ability and this is sufficient for entire expansion and shrinkage.

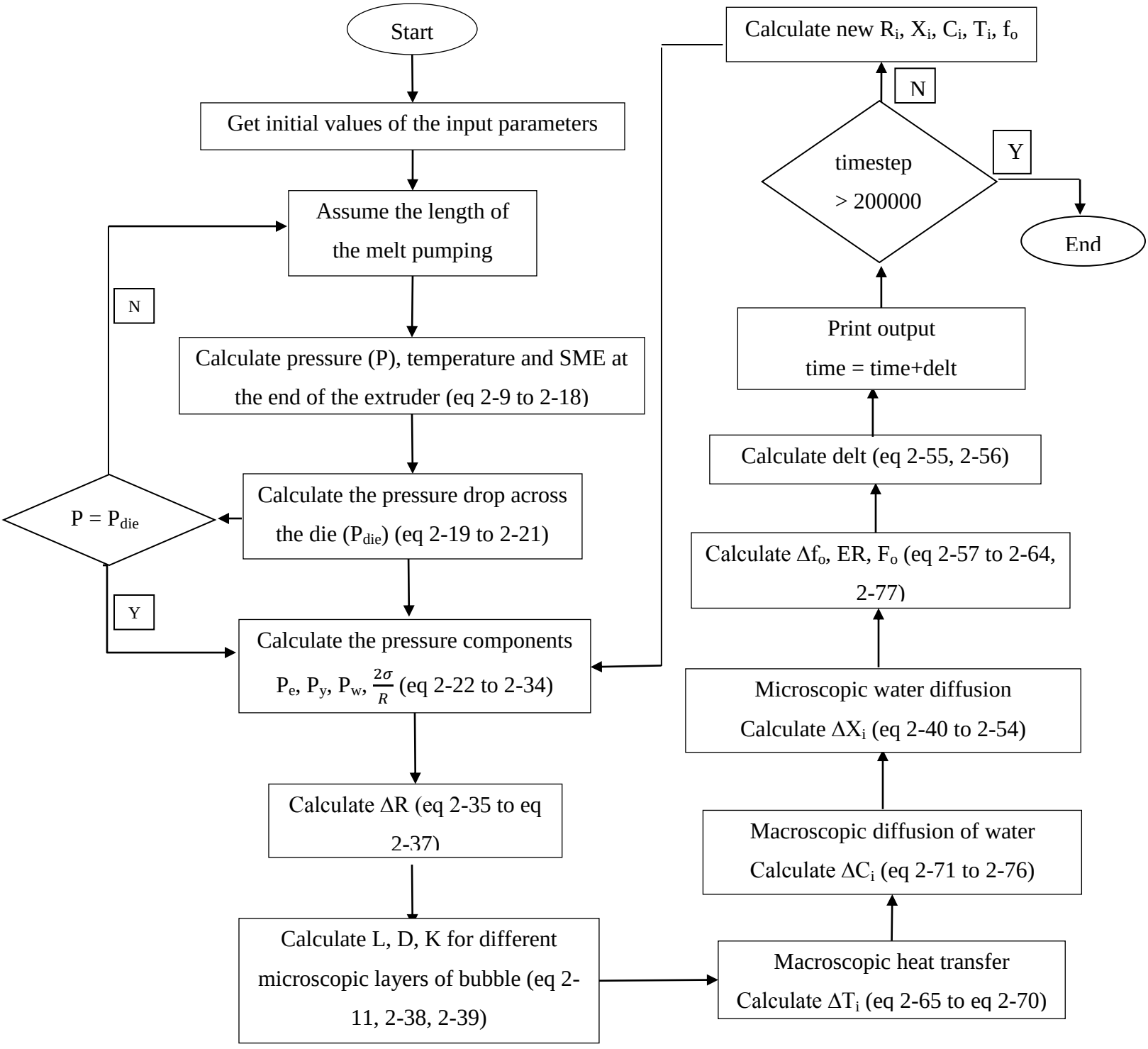

Figure 2-5 Algorithm for the mathematical model

2.3.7 Methodology

2.3.7.1 Extrusion run

Degermed corn meal purchased from Bunge (Atchison, KS) was used for production of corn puffs. The corn puffs were extruded using a pilot scale twin screw extruder (TX-52, Wenger Manufacturing, Sabetha, KS) with a differential diameter pre-conditioning cylinder. The extruder had a screw diameter of 52 mm and L/D ratio of 19:1. The screw profile and the barrel temperatures used were reported in Figure 2-6. A 3x2 factorial design was used with 3 in-barrel moisture contents (19%, 23.5%, 28% (db)) and two screw speeds (250 rpm and 330 rpm). The notations used for this treatments are shown in Table 2-2. Extrusion conditions were allowed to stabilize for ~10 minutes. The product from each treatment was collected for about 10 minutes. The raw material feed rate was maintained at 110 kg/h. There was no water or steam added in the preconditioner. The water was added only in the extruder.

Table 2-2 Notations for treatments

Treatment Notation	Moisture content (d.b.) %	Screw speed (RPM)
M.C. LO, RPM LO	19	250
M.C. LO, RPM HI	19	330
M.C. MD, RPM LO	23.5	250
M.C. MD, RPM HI	23.5	330
M.C. HI, RPM LO	28	250
M.C. HI, RPM HI	28	330

Head Number	1	2	3	4
Barrel Temperature (^{o}C)	50	60	70	90

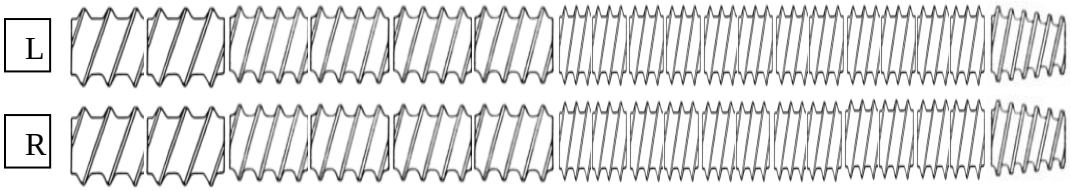

Figure 2-6 Screw profile

Element No:

1 = SE[b]-2-F-78; 2 = SE-2-F-78; 3 = SE-2-3/4-78; 4 = SE-2-3/4-78; 5 = SE-2-3/4-78;

6 = SE-2-3/4-78; 7 = SE-2-1/2-78; 8 = SE-2-1/2-78; 9 = SE-2-1/2-78; 10 = SE-2-1/2-78;

11 = SE-2-1/2-78; 12 = SE-2-1/2-52 and 13 = SE (conical)-2-3/4-78.[c]

[a]Right shaft elements are single flighted.

[b]SE = Screw element

Numbers:

1st – Number of flights

2nd – Relative pitch

3rd – Element length, mm

[c]All screw elements are forward and intermeshing

The die used was a circular die of 4.2 mm diameter. The dimensions of the die is given in Figure 2.7. The product was cut immediately after exiting the die with a face-mounted flex knife (6 blades) rotating at 539 rpm. The extrudates were dried in a dual pass dryer (Wenger Manufacturing, Sabetha, Kansas) at 212^{0} F for 15 minutes. Samples were collected at die exit as well as exit off the dryer.

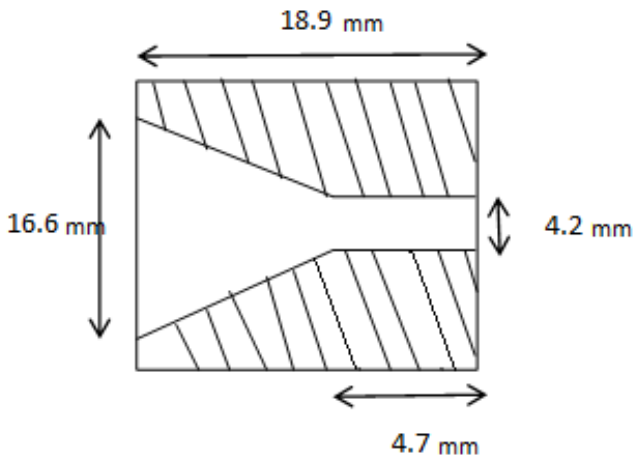

Figure 2-7 Dimensions of die used for extrusion

2.3.7.2 X-ray microtomography

For determining the microstructure parameters i.e. average pore radius and cell wall thickness, representative samples were collected from each treatment were selected for image analysis. A desktop X-ray microtomography imaging system (Model 1072, 20-100 kV/0-250 µA, SkyScan, Aartselaar, Belgium) was used to scan the samples. A set of two-dimensional virtual slices were obtained after reconstruction for each sample. Image analysis software was used to calculate microstructural parameters such as average pore radius and cell wall thickness based on measurement of 2-D features from each slice.

2.3.7.3 Specific mechanical energy

Specific mechanical energy (SME) was calculated experimentally using eqn 2-78

$$\mathrm{SME}\left(\frac{\mathrm{KJ}}{\mathrm{kg}}\right) = \frac{\left(\frac{\tau - \tau_o}{100}\right)}{\dot{m}} \times \frac{N}{N_r} \times P_r \qquad (2\text{-}78)$$

where τ is the % motor load torque, τ_o is the no load torque %, N is the screw speed of extruder, N_r is the rated screw speed (336 rpm), P_r is the rated motor power (22.37 kW) and $\dot{m}$ is the mass flow rate (kg/s).

2.3.7.4 Expansion ratio

The Expansion ratio (ER) is the ratio of the extrudate cross-sectional area to the die orifice cross sectional area, and was calculated using equation 2-79

$$ER = \frac{D_e^2}{d_{ex}^2} \tag{2-79}$$

where D_e is the extrudate diameter measured using vernier calipers and d_{ex} is the exit diameter of the die.

The video of the product extruded out of the die was recorded using the videocamera. The maximum expansion ratio of the extrudate was obtained by using pixelruler and calculating the maximum diameter from the video.

2.3.8 Results and Discussion

Predicted expansion ratio, die temperature, die pressure and average pore radius and cell wall thickness for each of the final extrudates were compared with experimental data at different moisture contents and screw speeds to validate the model. Confidence interval approach was used to compare the predicted resulted with the experimental results and the confidence interval percentage used was 95%. This approach signifies whether the experimental and predicted results are statistically different or same.

2.3.8.1 Pressure, Temperature and Energy inside the extruder

The comparisons between predictions and experimental values of Temperature at die, Pressure at die and Specific Mechanical Energy are shown in Fig 2-8 to 2-10 respectively. The difference between experimental and simulated values of temperature at die, pressure at die and specific

mechanical energy was statistically not different at level 0.05.

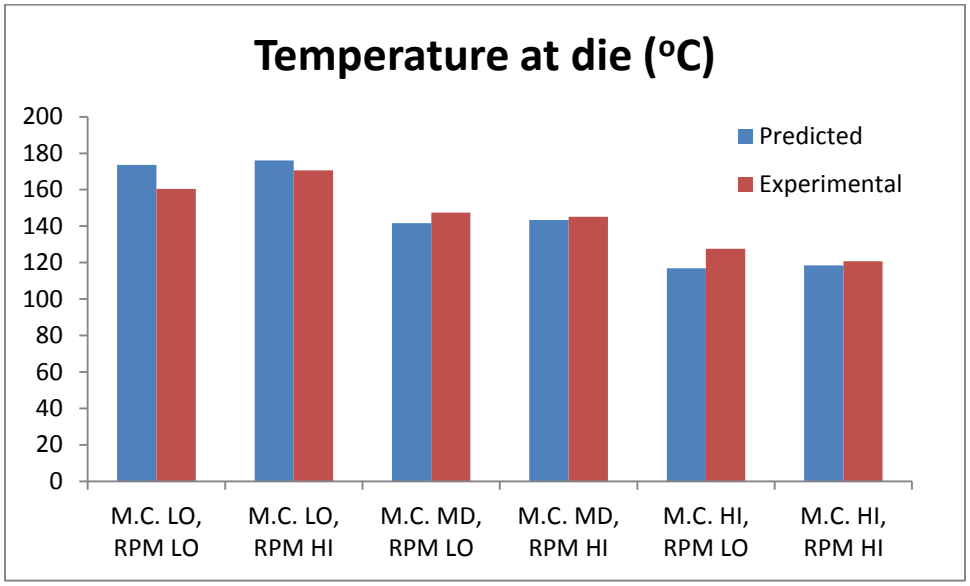

Figure 2-8 Experimental and predicted die temperature comparison

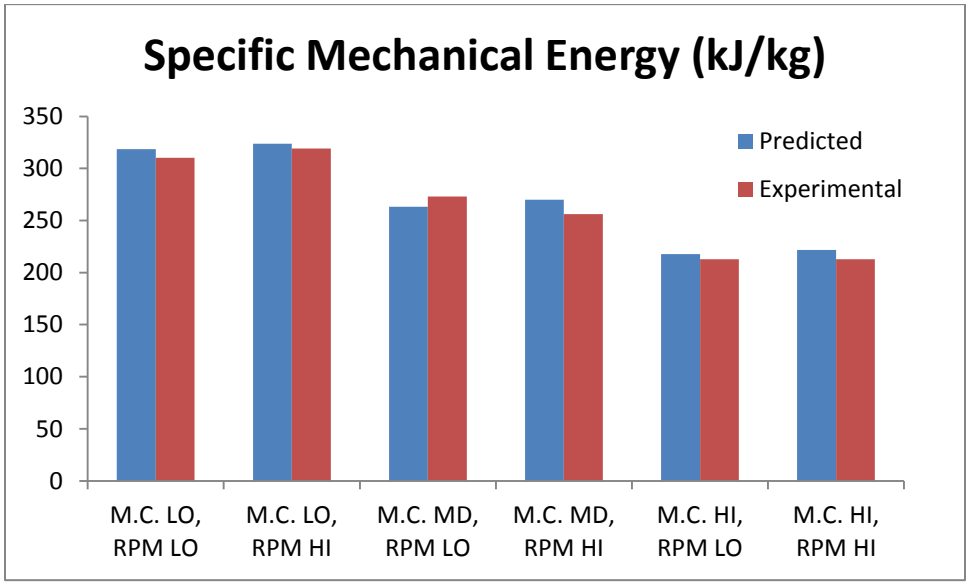

Figure 2-9 Experimental and predicted specific mechanical energy comparison

Simulated results (Figure 2-8, 2-9) show that SME and temperature at die decrease with the increase in moisture. This is due to the decrease in viscosity of melt with increase in moisture thus decreasing the SME and die temperature. Also the simulated results showed that SME and Die temperature increased with increase in screw speed. This is due to greater shear generated due to higher screw speed. Die pressure decreased with increase in screw speed (Figure 2-10) due to quick conveying of raw materials and thus reducing the fill in the barrel.

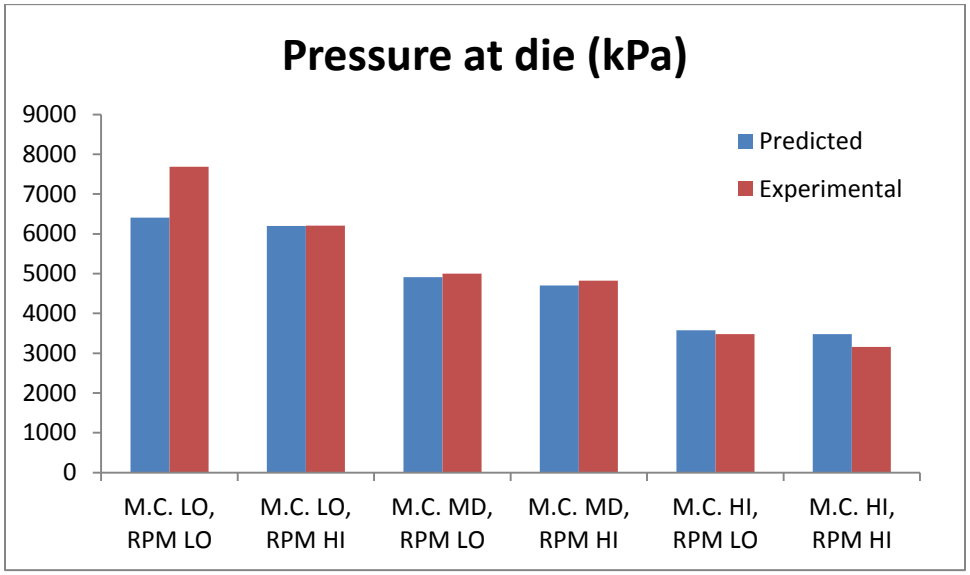

Figure 2-10 Experimental and predicted die pressure comparison

2.3.8.2 Bubble growth

Figure 2-11 gives the growth and shrinkage of bubble with time of exit from the die. The bubble grows very slowly as soon as it exits the die and very rapidly at the end of expansion. As the vapor pressure decreases due to fall in temperature, the vapor pressure inside the bubble becomes less than the outer pressure and the bubble starts shrinking causing the shrinkage of the extrudate as well. Also, the bubble ruptures and becomes an open cell during expansion. The open cells lose their ability to expand and shrink.

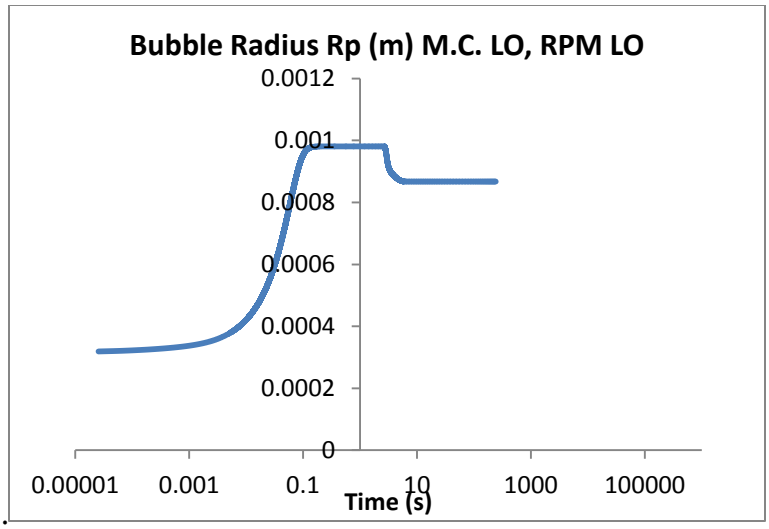

Figure 2-11 Bubble radius versus time for treatment M.C. LO, RPM LO

The experimental average bubble radius and cell wall thickness were obtained from X-ray microtomography. The comparisons between predictions and experimental values of average pore radius and cell wall thickness are shown in Fig 2-12 and Fig 2-13 respectively. The trend shows that the average bubble radius decreases in increase in moisture and increases with increase in screw speed. The increase in moisture decreases the die temperature and hence the bubble radius decreases. Increase in screw speed leads to more die temperature and thus increases the bubble radius. The difference between experimental and simulated values of bubble radius was statistically different at level 0.05.

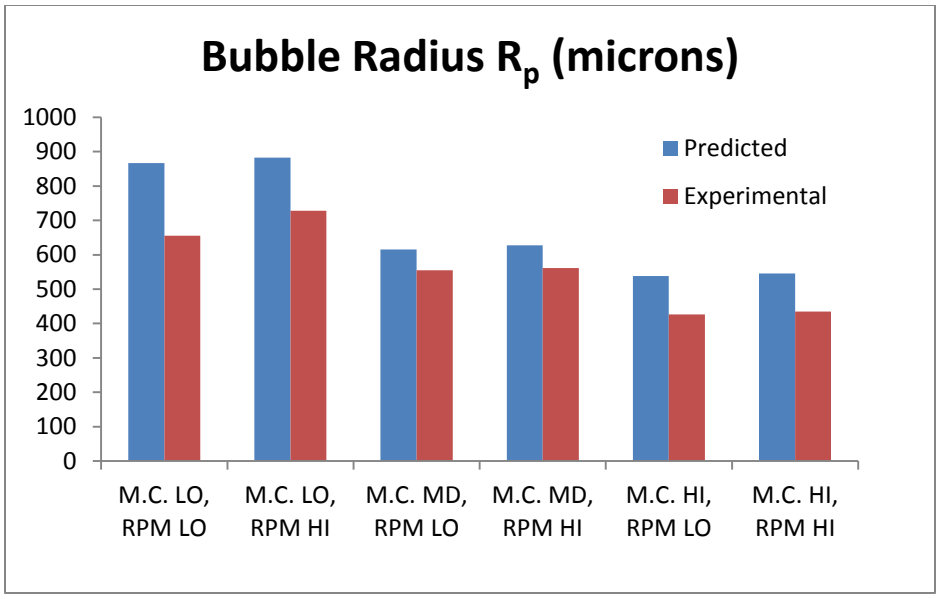

Figure 2-12 Experimental and predicted bubble radius comparison

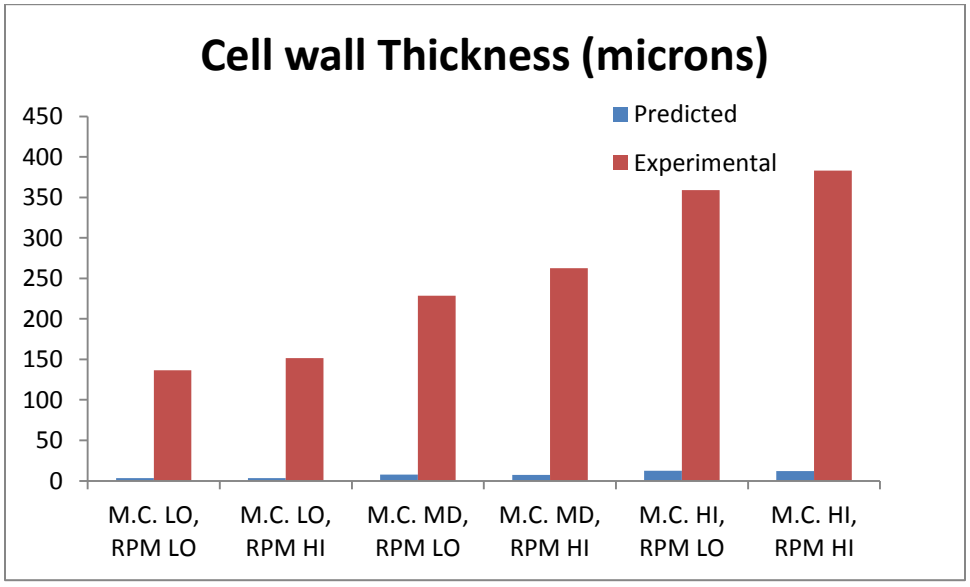

Figure 2-13 Experimental and predicted cell wall thickness comparison

The same trend was observed in experimental and simulated cell wall thickness. Cell wall thickness increases with increase in moisture because increase in moisture leads to small bubble radius. But the simulated cell wall thickness obtained for all the treatments were very low

compared to the experimental cell wall thickness. The difference between experimental and simulated values of cell wall thickness and bubble radius was statistically different at level 0.05. This can be due to the high nucleation density used (27500 bubbles/ cm^3 of unexpanded melt) which causes very low cell wall thickness due to the high number of bubbles. A proper nucleation density and rheological correlation for viscosity is important for studying the dynamics of the bubble and cell wall thickness needs to be further investigated.

2.3.8.3 Expansion ratio

The change in expansion ratio of the extrudate with time is shown in Fig 2-14. The product grows slowly as soon as it exits the die and increases rapidly at the end of expansion. The figure shows the maximum expansion ratio and the final expansion ratio after shrinkage. This can be used to validate with the data obtained from extrusion run.

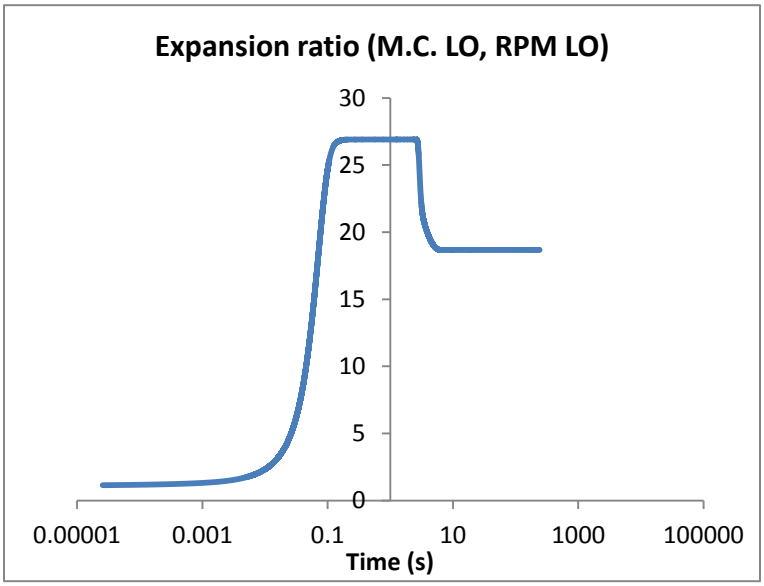

Figure 2-14 Expansion ratio versus time for treatment M.C. LO, RPM LO

The comparison between the predicted and experimental expansion ratio (both maximum and final expansion ratio) are shown in Fig 2-15, Fig 2-16

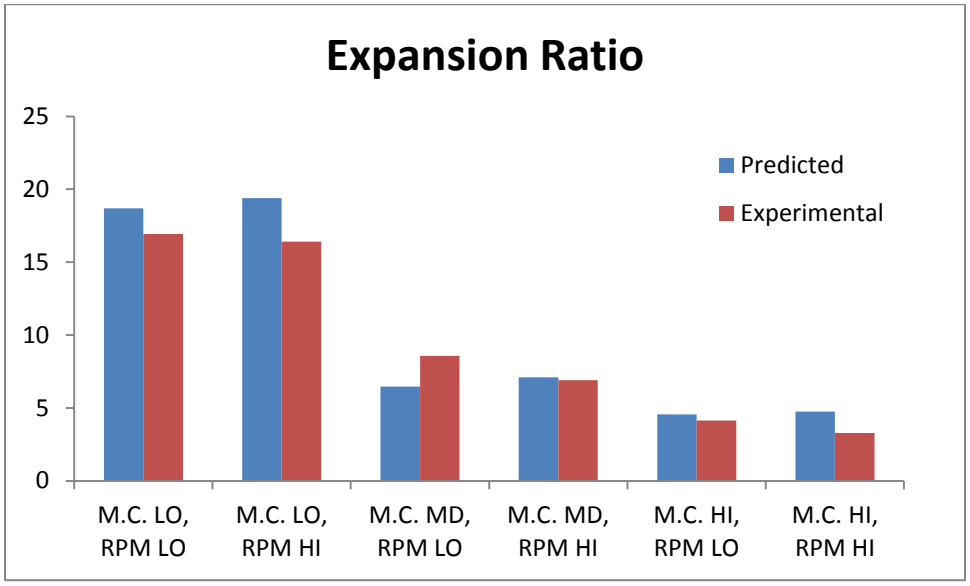

Figure 2-15 Experimental and predicted expansion ratio comparison

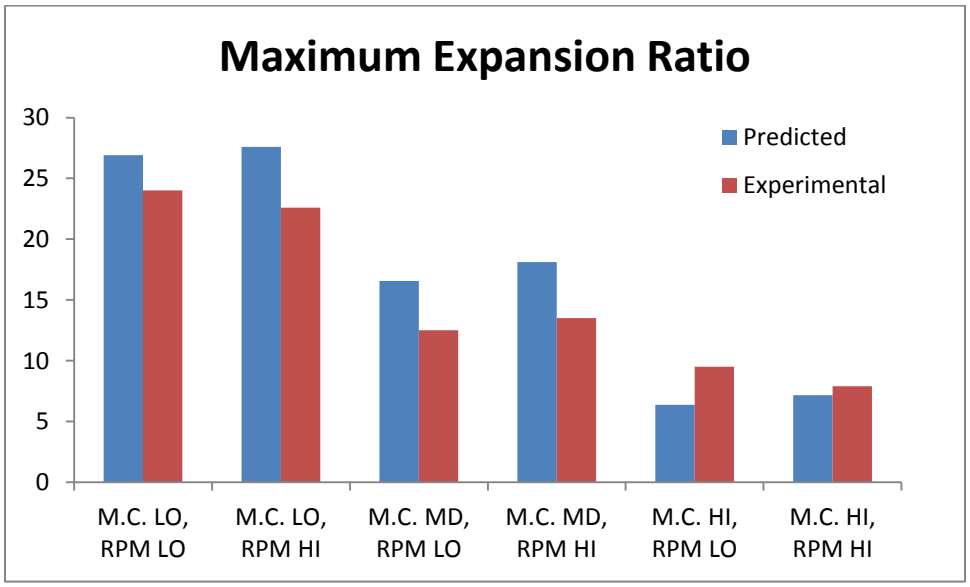

Figure 2-16 Experimental and predicted maximum expansion ratio comparison

The difference between experimental and simulated values of temperature at die, pressure at die and specific mechanical energy was statistically not different at level 0.05. The trend in

simulated results show that the expansion ratio decreases with increase in moisture content and increases with increase in screw speed as expected.

2.3.8.4 Temperature fall in extrudate

Fall in temperature of the extrudate is caused due to convection with the atmosphere as well as evaporation of water. As the bubble expands, water diffuses into the bubble and evaporates. Latent heat of vaporization causes the drop in energy which leads to drop in temperature. The temperature profile of the extrudate after it exits the die is shown in Fig 2-17

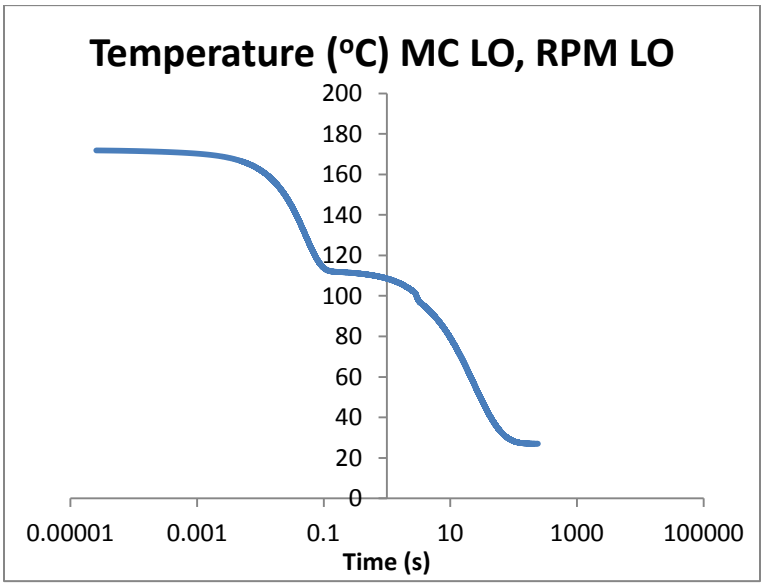

Figure 2-17 Temperature after exiting the die versus time for treatment M.C. LO, RPM LO

2.3.8.5 Literature comparison

Apart from the experimental validation of the mathematical model, the results from mechanistic model were compared with the literature values for better understanding. The literature values for expansion ratio of corn-based expansion products (Table 2-3) ranged from 3-19, depending

on the formulation and processing conditions which is in the same range of the value for expansion ratio predicted by the mathematical model (4.5-19.4).

Table 2-3 Literature comparisons for expansion ratio of corn based expanded products at different processing conditions

Reference	Material	Moisture content (db)	Screw speed (RPM)	Expansion ratio
Chinnaswamy and Hanna (1988)	Corn starch	15-40%	80-200	3.8-16.1
Karkle et al. (2012)	Corn flour	21-33%	350	5.9-10.5
de Mesa et al. (2009)	Corn starch	28.2 %	230-330	17.5-19
Anton et al. (2009)	Corn starch	28.2%	150	6.45
Desrumaux et al. (1998)	Corn grits	22.5%	130-200	9.14-12.8
Ahmed (1999)	Corn grits	22%	200	3
Mezreb et al. (2003)	Corn flour	-	200-500	7.6-11.8

For microscopic model or cellular architecture parameters (cell size, cell wall thickness), the values obtained from the mathematical model are compared with literature values (Table 2-4) for better understanding. It can be observed that the range of predicted (538-882 microns) and experimental values (435-728 microns) obtained for the cell size is in the same range for some of the values of the cell sizes obtained from literature. Also, the experimental values obtained for cell wall thickness (68.3-191.5 microns) is in the same range of the cell wall thickness obtained from literature (36-312 microns) although the predicted values of the cell wall thickness is very less (3.4-10.1 microns).

Table 2-4 Literature comparison for microstructure of corn based expanded products at different processing conditions

Reference	Material	Moisture content (db)	Screw speed (RPM)	Cell size (Radius) (microns)	Cell wall thickness (microns)	Bubble number density (cells/cm^3 expanded product)
Karkle et al. (2012)	Corn flour	21-33%	350	375-525	90-165	-
Cheng et al. (2007)	Corn starch	29-37%	300	785-1470	36-80.5	7-45
Trater et al. (2005)	Corn starch + 5% WPC	35-51%	-	575-850	65-75	2100-3400
Agbisit et al. (2007)	Corn starch	30-41%	200-400	1035-3160	65-125	18-146
Babin et al. (2007)	High amylose maize starch	25%	-	1650-1900	176.5-312	-
Barrett (1992)	Corn meal	17.6-25%	300-400	726-1052	-	-

Some of the input parameters of the microscopic model (Initial bubble radius, initial bubble density) are compared with literature in Table 2-5 for better idea.

Table 2-5 Literature comparison of some of the input parameters of microscopic model

Reference	Initial radius of bubble R_o (microns)	Initial radius of domain L_o (microns)	Initial bubble density N_{cell} (cells/cm^3 of unexpanded melt)	Reason
Wang et al. (2005)	650	1000	240	$R_o = (\frac{3}{4\pi} * \frac{(1+X_{wo})}{N_{bubble}\rho} * \frac{\epsilon_o}{1-\epsilon_o})^{\frac{1}{3}}$
Schwartzberg et al. (1995)	0.25	7.4	$5*10^9$	
Lach (2006)	5	320	500000	Assumed
Cisneros and Kokini (2002)	220-900	-	300-34550	
Fan et al. (2012)	100	200	-	
Alavi et al. (2003)	5	39.8	5000000	

Table 2-6 List of symbols and their meanings

A_i	Interfacial area between layers i and i+1 in microscopic shells (m^2)
a_w	Water activity for given moisture content at bubble surface
C_j	Concentration of water in the j_{th} shell of the macroscopic shells (kg/kg dry matter)
C_p	Specific heat (kJ/kg K)
D_w	Diffusivity of water in cell wall (m^2/s)
D_{eff}	Effective bulk diffusivity of water in porous extrudate (m^2/s)
D_{wi}	Diffusivity of water in each layer of the starch matrix (m^2/s)
d_{en}	Die diameter at entrance of die (m)
d_{ex}	Die diameter at exit of die (m)
D	Diameter of screw (m)
D_i	Internal screw diameter (m)
e	Screw flight thickness (m)
f_o	Fraction of number of open cells
F_D	Shape factor for drag flow
F_o	Fraction of volume of open cells
F_P	Shape factor for pressure flow
h	Screw channel depth (m)
K	Consistency coefficient of melt (kPa s^n)
K_c	K at the innermost surface of the pore (kPa s^n)
K_s	K at the outermost surface of the pore (kPa s^n)
K_{xc}	Mass transfer coefficient of water in starch matrix
L	Radius of domain (m)
L_d	Extruder nozzle length (m)
L_{d1}	Extruder nozzle dimension (m)
Lv	Channel width (m)
M	Mass of dry solids in the domain (kg)
m_f	Mass flow rate (kg/s)
n	Flow behavior index
n_f	Number of threads
N	Screw speed (rps)
N_{mi}	Number of spherical shells used for microscopic model
N_{bubble}	Bubble nucleation density (bubbles/m^3 of unexpanded material)
P_w	Pressure exerted due to water vapor inside the bubble (Pa)
P_{wsat}	Saturated water vapor pressure at temperature T (Pa)
P_a	Atmospheric pressure (Pa)
P_e	Elastic stress (Pa)
P_y	Yield stress (Pa)
Q	Mass of water vapor in pore (kg)
Q_v	Volumetric flow rate (m^3/s)
R	Bubble radius (m)
S_w	Average tensile stress in cell wall (Pa)
S_f	Cell wall failure stress (Pa)
S_m	Coefficient in S_r versus T correlation (kPa)
S_r	Term in S_f versus X_a correlation (kPa)

SME	Specific mechanical energy (kJ/kg)
t	Pitch (m)
T	Temperature (K)
T_{ref}	Reference temperature (K)
W	Cell wall thickness of domain (m)
X_w	Moisture content (dry basis)
X_a	Average moisture content across all layers (dry basis)
X_C	Moisture content at the innermost surface of the pore (dry basis)
X_i	Moisture content at i^{th} shell of the bubble (dry basis)
X_S	Moisture content at the outermost surface of the pore (dry basis)
ρ	Density of melt (kg/m^3)
ρ_{dry}	Density of dry unexpanded melt (kg/m^3)
σ	Surface tension at pore-shell interface (N/m)
γ	Shear rate (s^{-1})
μ	Melt viscosity (kPa s)
υ	Specific volume of water vapor (m^3/kg)
Φ	Screw pitch angle
λ	Latent heat of vaporization (kJ/kg)
Ψ	Spread factor in open cell fraction distribution
ϵ	Porosity
ζ	Tortuosity
τ_o	Flow yield stress (kPa)
β_f	Coefficient in $\tau_o$correlation
β_s	Coefficient in S_f versus X_a correlation
ΔM	Mass of dry solids per layer of the bubble (kg)
ΔP	Pressure difference driving expansion
ΔP_E	Increase in pressure inside the extruder due to Δx thickness of screw
ΔQ	Change in Q in timestep Δt
ΔR	Change in bubble radius in timestep Δt (m)
Δt	Value of timestep
ΔT_E	Increase in temperature inside the extruder due to Δx thickness of screw

2.4 References

Achanta, S., Okos, M.R., Cushman, J.H., & Kessler, D.P. (1997). Moisture transport in shrinking gels during saturated drying. Aiche Journal, 43(8), 2112-2122.

Agbisit, R., Alavi, S., Cheng, E., Herald, T & Trater, A. (2007). Relationships between microstructure and mechanical properties of cellular cornstarch extrudates. Journal of Texture Studies, 38, 199-219.

Ahmed, Z.S. (1999). Physico-chemical, structural and sensory quality of corn-based flax-snack. Nahrung, 43, 253-258.

Alavi, S.H., Rizvi, S.S.H., & Harriott, P. (2003a). Process dynamics of starch-based microcellular foams produced by supercritical fluid extrusion. I: model development. Food Research International, 36, 309-319.

Alavi, S.H., Rizvi, S.S.H., & Harriott, P. (2003b). Process dynamics of starch-based microcellular foams produced by supercritical fluid extrusion. II: Numerical simulation and experimental evaluation. Food Research International, 36(4), 321-330.

Alvarez-Martinez, L., Kondury, K.P., & Harper, J.M. (1988). A general model for expansion of extruded products. Journal of Food Science, 53, 609-15.

Amon, M. & Denson, C.D. (1984). A study of the dynamics of foam growth: analysis of the growth of closely spaced spherical bubbles. Polymer Engineering and Science, 24, 1026-1034.

Anton, A.A., Fulcher, R.G. & Arntfield, S.D. (2009). Physical and nutritional impact of fortification of corn starch-based extruded snacks with common bean (Phaseolus vulgaris L.) flour: Effects of bean addition and extrusion cooking. Food Chemistry, 113, 989-996.

Arefmanesh, A., Advani, S.G., & Michaelides, E.E. (1990). A numerical study of bubble growth during low pressure structural foam molding process. Polymer Engineering and Science, 30(20), 1330-1337.

Arefmanesh, A., Advani, S.G., & Michaelides, E.E. (1992). Accurate numerical solution for mass diffusion-induced bubble growth in viscous liquids containing limited dissolved gas. International Journal of Heat and Mass Transfer, 35(7), 1711-1722.

Babin, P., Della Valle, G., Dendievel, R., Lourdin, D. & Salvo, L. (2007). X-ray tomography study of the cellular structure of extruded starches and its relations with expansion phenomenon and foam mechanical properties. Carbohydrate Polymers, 68, 329-340.

Barlow, E.J., & Langlois, W.E. (1962). Diffusion of gas from a liquid into an expanding bubble. IBM Journal of Research and Development, 6, 329-337.

Barrett, A.M. (1992). Cell size distributions of puffed corn extrudates. Journal of Food Science, 57, 146-148.

Bloksma, A.H., & Nieman, W. (1975). The effect of temperature on some rheological properties of wheat flour doughs. Journal of Texture Studies, 6, 343-361.

Bouzaza, D., Arhaliass, A., & Bouvier, J.M. (1996). Die design and dough expansion in low moisture extrusion-cooking process. Journal of Food Engineering, 29(2), 139-152.

Chen, C.M., & Yeh, A.I. (2000). Expansion of rice pellets: examination of glass transition and expansion temperature. Journal of Cereal Science, 32(2), 137-145.

Cheng, E.M., Alavi, S., Pearson, T., & Agbisit, R. (2007). Mechanical-acoustic and sensory evaluations of cornstarch-whey protein isolate extrudates. Journal of Texture Studies, 38, 473-498.

Chinnaswamy, R. and Hanna, M.A. (1988). Optimum extrusion-cooking conditions for maximum expansion of corn starch. Journal of Food Science, 53(3), 834-836.

Chiruvella, R.V., Jaluria, Y. & Karwe, M.V. (1996). Numerical simulation of the extrusion process for food materials in a single screw extruder. Journal of Food Engineering, 30(3), 449-467.

Cisneros, F.H. & Kokini, J.L. (2002). Effect of extrusion operating parameters on air bubble entrapment. Journal of Food Process Engineering, 25, 251-283.

Della Valle, G., Barres, C., Plewa, J., Tayeb, J., & Vergnes, B. (1993). Computer simulation of starchy products transformation by twin-screw extrusion. Journal of Food Engineering, 19(1), 1-31.

DellaValle, G., Vergnes, B., Colonna, P., & Patria, A. (1997). Relations between rheological properties of molten starches and their expansion behaviour in extrusion. Journal of Food Engineering, 31(3), 277-295.

de Mesa, N.J.E., Alavi, S., Singh, N., Shi, Y., Dogan, H. & Sang, Y. (2009). Soy protein-fortified expanded extrudates: Baseline study using normal corn starch. Journal of Food Engineering, 90, 262-270.

Desrumaux , A., Bouvier, J.M. & Burri, J. (1998). Corn grits particle size and distribution effects on the charactersitcis of expanded extrudates. Journal of Food Science, 63(5), 1-7.

Fan, J.T., Mitchell, J.R., & Blanshard, J.M.V. (1994). A computer simulation of the dynamics of bubble growth and shrinkage during extrudate expansion. Journal of Food Engineering, 23(3), 337-356.

Fan, J.T., Mitchell, J.R., & Blanshard, J.M.V. (1999). A model for the oven rise of dough during baking. Journal of Food Engineering, 41(2), 69-77.

Fan, X., Meng, Z., Zhou, J., Xu, W., Xiang, H. & Yang, G. (2012). Investigation of bubble growth in extrusion expansion of cornstarch with CFD method. International Journal of Food Engineering, 8, 1-19.

Geankoplis, C.J. (1993). Transport processes and unit operations. (3rd ed.). Geankoplis, Englewood Cliffs, NJ: Prentice Hall.

Guy, R.C.E., & Horne, A.W. (1988). Extrusion and co-extrusion of cereals, in food structure - its creation and evaluation, Blanshard, J.M.V., & Mitchell, J.R., editors. Butterworths: London, 331-349.

Huang, H., & Kokini, J.L. (1999). Prediction of dough volume development which considers the biaxial extensional growth of cells, in Bubbles in food, Niranjan, K. Editor., Eagan press: St Paul, Minnesota. p. 113-120.

Jiang, Q. (2008). Modeling flow, melting, solid conveying and global behavior in intermeshing counter-rotating twin screw extruders. Ph.D. thesis. University of Akron, Akron.

Joshi, K., Lee, J.G., Shafi, M.A., & Flumerfelt, R.W. (1998). Prediction of cellular structure in free expansion of viscoelastic media. Journal of Applied Polymer Science, 67(8), 1353-1368.

Karkle, E.L., Alavi, S., & Dogan, H. (2012). Cellular architecture and its relationship with mechanical properties in expanded extrudates containing apple pomace. Food Research International, 46, 10-12.

Kirby, A.R., Ollett, A.L., Parker, R., & Smith, A.C. (1988). An experimental study of screw configuration effects in the twin-screw extrusion - cooking of maize grits. Journal of Food Engineering, 8(4), 247-272.

Kokini, J.L., Chang, C.N., & Lai, L.S. (1991). The role of rheological properties on extrudate expansion. Food Extrusion Science and Technology, 631-652.

Lach, L. (2006). Modelling vapour expansion of extruded cereals. Ph.D. thesis. Ecole Polytechnique federale de Lausanne, Lausanne.

Lai, L.S., & Kokini, J.L. (1991). Physicochemical changes and rheological properties of starch during extrusion (a review). Biotechnology progress, 7(3), 251-266.

Lai, L.S., & Kokini, J.L. (1992). Estimation of viscous heat effects in slit flows of 98% amylopectin (Amioca), 70% amylose (Hylon 7) corn starches and corn meal during expansion. Journal of Food Engineering, 16(4), 309-318.

Mezreb, K., Gouilleux, A., Ralainirina, R., Queneudec, M. (2003). Application of image analysis to measure screw speed influence on physical properties of corn and wheat extrudates. Journal of Food Engineering, 57(2), 145-152.

Mikic, B.B., Rohsenow, W.M., & G. P., (1970). On bubble growth rates. International Journal of Heat and Mass Transfer, 13, 657-666.

Mitchell, J.R., Fan, J., & Blanshard, J.M.V. (1998). Simulation of bubble growth in heat processed cereal systems, in Bubbles in food, Niranjan, K. Editor, Eagan press:St Paul, Minnesota, USA. p. 107-112.

Padmanabhan, M. (1995). Measurement of extensional viscosity of viscoelastic liquid foods. Journal of Food Engineering, 25, 311-327.

Pai, V., & Favelukis, M. (2002). Dynamics of spherical bubble growth. Journal of Cellular Plastics, 38(5), 403-419.

Ramesh, N.S. (1998). Bubble growth in thermoplastic foam extrusion- Porous, cellular and microcellular materials. American Society of Mechanical Engineers, Materials Division, 82, 71-74.

Ramesh, N.S., & Malwitz, N. (1999). A non-isothermal model to study the influence of blowing agent concentration on polymer viscosity and gas diffusivity in thermoplastic foam extrusion. Journal of Cellular Plastics, 35(3), 199-209.

Rauwendaal, C. (1986). Throughput-pressure relationships for power law fluids in single screw extruders. Polymer Engineering and Science, 26, 1240-1244.

Rossen, J.L. & Miller, R.C. (1973). Food extrusion. Food Technology, 46-53.

Schwartzberg, H.G., Wu, J.P.C., Nussinovitch, A., & Mugerwa, J. (1995). Modelling deformation and flow during vapor-induced puffing. Journal of Food Engineering, 25(3), 329-372.

Senouci, A. & Smith, A.C. (1988). An experimental study of food melt rheology. I. Shear viscosity using a slit die viscometer and a capillary rheometer. Rheological Acta, 27, 546-554.

Shafi, M.A., & Flumerfelt, R.W. (1997). Initial bubble growth in polymer foam processes. Chemical Engineering Science, 52(4), 627-633.

Shafi, M.A., Joshi, K., & Flumerfelt, R.W. (1997). Bubble size distributions in freely expanded polymer foams. Chemical engineering science, 52(4), 635-644.

Shafi, M.A., Lee, J.G., & Flumerfelt, R.W. (1997). Prediction of cellular structure in free expansion polymer foam processing. Polymer Engineering and Science, 36(14), 1950-1959.

Shah, P., Campbell, G.M., McKee, S.L., & Rielly, C.D. (1998). Proving of bread dough: modelling the growth of individual bubbles. Food and Bio-products Processing, 76(2), 73-79.

Shimiya, Y., & Yano, T. (1987). Diffusion-controlled shrinkage and growth of an air bubble entrained in water and in wheat flour particles. Agricultural and Biological Chemistry, 51(7), 1935-1940.

Shimiya, Y., & Yano, T. (1988). Rates of shrinkage and growth of air bubbles entrained in wheat flour dough. Agricultural and Biological Chemistry, 52(11), 2879-2883.

Shimoda, M., Tsujimura, I., Tanigaki, M., & Ohshima, M. (2001). Polymeric foaming simulation for extrusion processes. Journal of Cellular Plastics, 37(6), 517-536.

Steffe, J.F. (1992). Rheological methods in food process engineering. E.Lansing, MI: Freeman Press

Street, J.R. (1968). The rheology of phase growth in elastic liquids. Transactions of the Society of Rheology, 12(1), 103-131.

Street, J.R., Fricke, A.L., & Reiss, L.P. (1971). Dynamics of phase growth in viscous, non-newtonian liquids. Industrial & Engineering Chemistry Fundamentals, 10(1), 54-64.

Tayeb, J., Vergnes, B.& DellaValle, G. (1989). A basic model for a twin-screw extruder. Journal of Food Science, 54, 1047-1056.

Trater, A.M., Alavi, S., & Rizvi, S.S.H. (2005). Use of non-invasive X-ray microtomography for characterizing microstructure of extruded biopolymer foams. Food Research International, 38, 709-719.

Venerus, D.C. (2001). Diffusion-induced bubble growth in viscous liquids of finite and infinite extent. Polymer Engineering and Science, 41(8), 1390-1398.

Venerus, D.C., & Yala, N. (1997). Transport analysis of diffusion-induced bubble growth and collapse in viscous liquids. Aiche Journal, 43(11), 2948-2959.

Venerus, D.C., Yala, N., & Bernstein, B. (1997). Analysis of diffusion-induced bubble growth in viscoelastic liquids. Journal of Non-Newtonian Fluid Mechanics, 75(1), 55-75.

Vergnes, B., Della Valle, G., & Tayeb, J. (1993). A specific slit die rheometer for extruded starchy products- design, validation and application to maize starch. Rheological Acta, 32(5), 465-476.

Vergnes, B., & Berzin, F. (2006). Modeling of reactive systems in twin screw extrusion: challenges and applications. Comptes Rendus Chimie, 9, 1409-1418.

Wang, L., Ganjyal, G.M., Jones, D.D., Weller, C.L. & Hanna, M.A. (2005). Bubble growth dynamics in starch-based foams. Advances in Polymer Technology, 24, 29-45.

Yacu, W.A. (1985). Modeling a twin screw co-rotating extruder. Journal of Food Process Engineering, 8(1), 1-21.

Yang, W.J. & Yeh, H.C. (1966). Theoretical study of bubble dynamics in purely viscous fluids. Aiche Journal, 12(5), 927-931.

Chapter 3 - Stochastic study of flow and expansion of starch-based melts during extrusion

3.1 Introduction

With the increase in population, and also due to changes in the consumer preferences a revolution took place in the food industry to produce different varieties of products with better quality. In the production of different variety food products, along with different other methods, extrusion cooking played an important role especially in the production of expanded products such as breakfast cereal, snack food, pet food etc. Extrusion cooking not only has its impact on the increment of production but also holds great potential in the incorporation of difficult biomaterials such as fiber besides maintaining organoleptic quality of the food product. Mathematical modeling acts as an effective tool in understanding the fundamental concepts of the process and also aids in simulating the outcome of a process without actually performing the experiment (Vergnes et al., 2006). The purpose of the mathematical model in the food process is to describe the heat and mass transfer occurring in the product as accurately as possible. Modeling of food extrusion process is a complex process because of the heterogenous properties of the food materials and their phase transitions are not well-defined. The extrusion process involves simultaneous mass and heat transfer along with other physico-chemical processes such as evaporation of water, protein denaturation, starch gelatinization etc.

There are two types of uncertainties in modeling the heat and mass transfer systems (Feyissa et al., 2012)

1) Uncertainties due to the model assumptions made to simplify the model development where only crucial physical phenomena are observed and the other phenomena are ignored or assumed to cause no effect. This often leads to the variation between the

predicted model dynamics and reality. This kind of uncertainty is called as Subjective uncertainty as it is related to the model assumptions or in other words, structure of the model.

2) Uncertainties due to uncertainty in the values of the parameters used in the model. This uncertainty may occur due to the poor understanding of the phenomena or the values of these parameters are not available in literature. Though there are methods (Dolan and Mishra (2012), Beck and Arnold (2007)) to estimate the parameters in the food processes which could address this issue to an extent; the uncertainties in values of parameters causes issues in the predictive models (Wong et al., 2006). This can be dealt by taking the uncertainty in input parameters into account and studying the effect of these uncertainties on the end product characteristics. The effect of uncertainties in input parameter on the end product was currently studied in the model.

Uncertainty and sensitivity analysis has been used in several applications such as quality assessment of composite indicators (Saisana et al., 2005), environmental models (Campolongo and Saltelli, 1997), ecological modeling (Cariboni et al., 2007), arterial blood flow and blood pressure models (Ellwein et al., 2008), data based mechanistic modeling in hydrology (Ratto et al., 2007), chemical models (Saltelli et al., 2005), process analytical technology applications (Sin et al., 2009). Uncertainty analysis helps in studying the effect of uncertainty of input parameters on uncertainty of output parameters whereas sensitivity analysis helps in knowing which input parameter affects output the most. There are two ways of sensitivity analysis methods (Sobol, 2001) – local sensitivity analysis method and global sensitivity analysis method. Local sensitivity analysis method involves studying the effect of small changes in input of one

parameter on the output at a time whereas global sensitivity analysis method involves studying the effect of changes in all the input parameters at the same time on the output. Though the local sensitivity analysis was used more frequently due to less computational requirement; global sensitivity analysis was currently used in this model as it involves the changes in all input parameters simultaneously.

Feyissa et al. (2012) studied the uncertainty and sensitivity analysis in a contact baking process. They used global sensitivity analysis method in the heat and mass transfer model of a contact baking process to study the effect of input parameters such as heat and mass transfer coefficients, evaporation rate parameters, thermo-physical parameter characteristics etc. and ranked the relative impact of each input parameter on the output. They used Monte-Carlo technique to study the uncertainty analysis.

In this study, the effect of variability of input parameters such as moisture content and screw speed on the output i.e. expansion ratio of the extrudate was observed. Data Acquisition System (DAQ) was used during the actual extrusion run to record water injection into the extruder and the screw speed.

3.2 Methodology

3.2.1 Mathematical model and input parameters

The mathematical model developed in Chapter 2 gives the pressure, temperature and energy profiles inside the extruder. It also explains the phenomena of expansion and shrinkage of bubbles after the extrudate exits from die and helps in obtaining the end product characteristics such as expansion radius, bubble radius, cell wall thickness etc. This model was used to study the effect of variability of input parameters on the output. The input parameters used for study was

in-barrel moisture content and screw speed and the effect of these parameters on expansion ratio can be observed using the Data Acquisition System (DAQ).

3.2.2 Extrusion run

Degermed corn meal purchased from Bunge (Atchison, KS) was used for production of corn puffs. The corn puffs were extruded using a pilot scale twin screw extruder (TX-52, Wenger Manufacturing, Sabetha, KS) with a differential diameter pre-conditioning cylinder. The extruder had a screw diameter of 52 mm and L/D ratio of 19:1. The screw profile and the barrel temperatures used were reported in Figure 3-1. A 3x2 factorial design was used with 3 in-barrel moisture contents (0.19, 0.235, 0.28 (db)) and two screw speeds (250 rpm and 330 rpm). The notations used for this treatments are shown in Table 3-1.

Table 3-1 Notations for treatments

Treatment Notation	Moisture content (d.b.) %	Screw speed (RPM)
M.C. LO, RPM LO	19	250
M.C. LO, RPM HI	19	330
M.C. MD, RPM LO	23.5	250
M.C. MD, RPM HI	23.5	330
M.C. HI, RPM LO	28	250
M.C. HI, RPM HI	28	330

Extrusion conditions were allowed to stabilize for ~10 minutes. The product from each treatment was collected for about 10 minutes. The raw material feed rate was maintained at 110 kg/h. There was no water or steam added in the preconditioner. The water was added only in the extruder.

Head Number	1	2	3	4
Barrel Temperature (^{o}C)	50	60	70	90

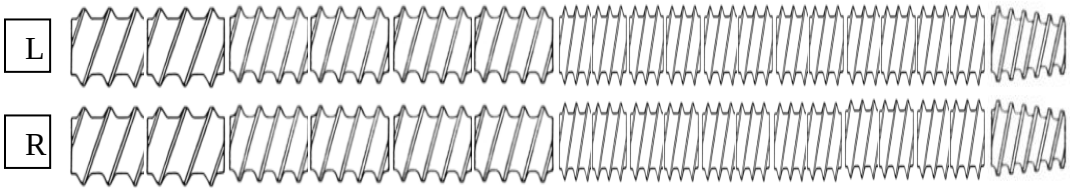

Figure 3-1 Screw profile

Element No:

1 = SE[b]-2-F-78; 2 = SE-2-F-78; 3 = SE-2-3/4-78; 4 = SE-2-3/4-78; 5 = SE-2-3/4-78;

6 = SE-2-3/4-78; 7 = SE-2-1/2-78; 8 = SE-2-1/2-78; 9 = SE-2-1/2-78; 10 = SE-2-1/2-78;

11 = SE-2-1/2-78; 12 = SE-2-1/2-52 and 13 = SE (conical)-2-3/4-78.[c]

[a]Right shaft elements are single flighted.

[b]SE = Screw element

Numbers:

1st – Number of flights

2nd – Relative pitch

3rd – Element length, mm

[c]All screw elements are forward and intermeshing.

The die used was a circular die of 4.2 mm diameter. The dimensions of the die is given in Figure 3-2. The product was cut immediately after exiting the die with a face-mounted flex knife (6 blades) rotating at 539 rpm. The extrudates were dried in a dual pass dryer (Wenger Manufacturing, Sabetha, Kansas) at 212^{0} F for 15 minutes. Samples were collected off the extruder as well as off the dryer.

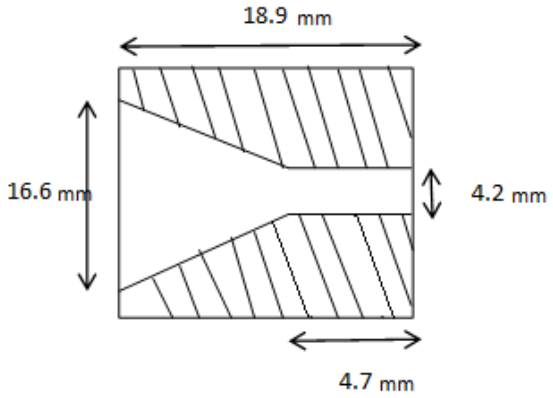

Figure 3-2 Dimensions of die used in extrusion

3.2.3 Data acquisition system (DAQ)

Data acquisition system was used during the extrusion run to record the extrusion processing conditions every second. This helps in understanding the variability of input parameters. Some of the parameters recorded by DAQ are water added into the extruder and screw speed. In-barrel moisture content was calculated from the water added into the extruder and feed rate. Fig 3-3 and Fig 3-4 shows the change in water added and screw speed every second during the extrusion run for treatment M.C. MD, RPM LO respectively.

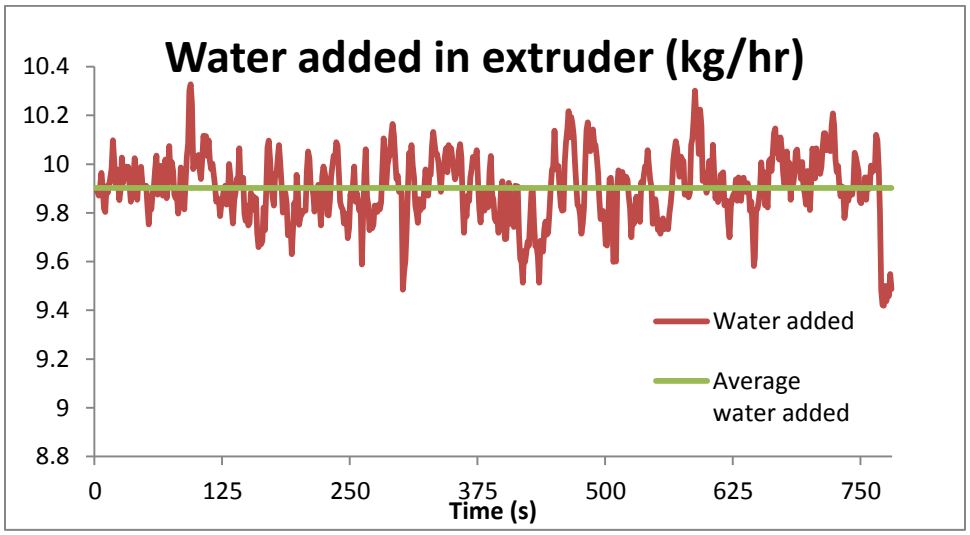

Figure 3-3 DAQ data for water added during extrusion for M.C. MD, RPM LO

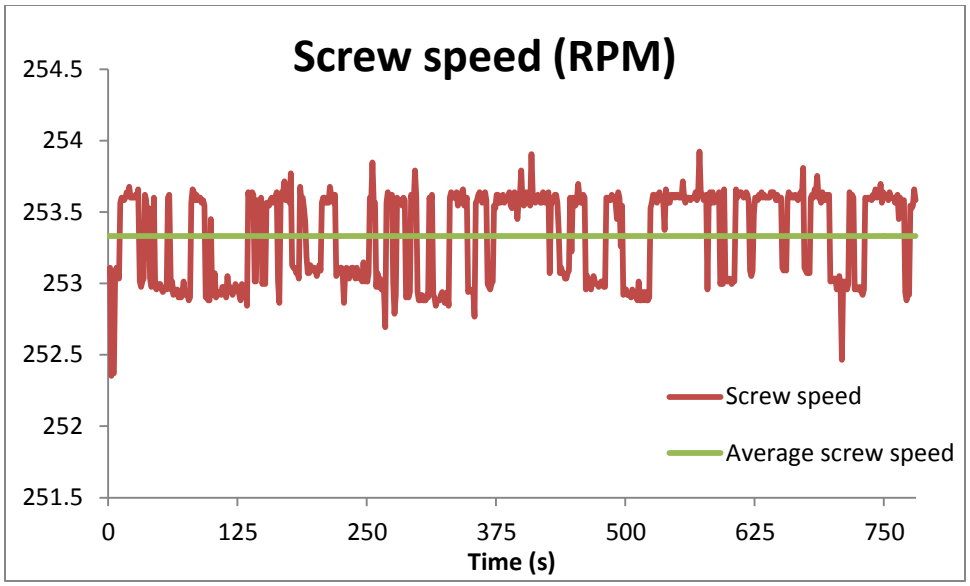

Figure 3-4 DAQ data for screw speed during extrusion for M.C. MD, RPM LO

3.2.4 Expansion ratio

The Expansion ratio (ER) is the ratio of the extrudate cross-sectional area to the die orifice cross sectional area, and was calculated using equation 3-1

$$ER = \frac{D_e^2}{d_{ex}^2} \tag{3-1}$$

where D_e is the extrudate diameter measured using vernier calipers and d_{ex} is the exit diameter of the die.

3.2.5 Monte-Carlo simulation

Though there are many techniques available for uncertainty analysis, Monte-Carlo simulation was used as it is the most effective way to analyze the uncertainty (Helton and Davis, 2003) and is the most reliable and effective technique (Sin et al., 2009). The steps involved in Monte-Carlo simulation are (Feyissa et al., 2012)

1) Uncertainty in input parameters
2) Sampling the uncertainty of input

3) Evaluation of model

4) Analysis of result – uncertainty of output

3.2.5.1 Uncertainty in input parameters

This step varies for each input parameter. If the input parameter is obtained from literature or assumption, coefficient of variation (CV) was assumed. High CV signifies more uncertainty of the input parameter whereas less CV signifies less uncertainty of the parameter. If the input paremeter is measured from experiments, the uncertainty range of the input parameters can be obtained from experimental data. In this study, we are studying the effect of uncertainty of moisture content and screw speed. DAQ measures water injection to extruder and screw second every second which was used to obtain the uncertainty of these input parameters.

3.2.5.2 Sampling the uncertainty of input

Random sampling was used to the sample the input parameters from the DAQ data. Random sampling is the most used type of probability sampling. 600 samples were selected from the input parameter data (DAQ data). In random sampling, each value of the input parameter has an equal probability to be selected for sampling. This value of the input parameter is selected independently of the values of other input parameters. The random selection is done using the random-number generator in MS-Excel. Thus, N random values of input parameters (screw speed, moisture content) were obtained from the sampling space.

3.2.5.3 Evaluation of model

The N random values of input parameters selected from the sampling space were used as the input to the mathematical model. The first set of input data gives the first simulated output and the second set of input data gives the second simulated output, and thereby N values of output

data was obtained using N random values of input parameters. This step takes the most time as there are so many computations involved.

3.2.5.4 Analysis of result – uncertainty of output

The uncertainty of output was obtained using the N values of output obtained in the previous step. It was represented by CV of the output data calculated by measuring the mean and standard deviation of the output.

The algorithm for stochastic modeling is shown in Figure 3-5

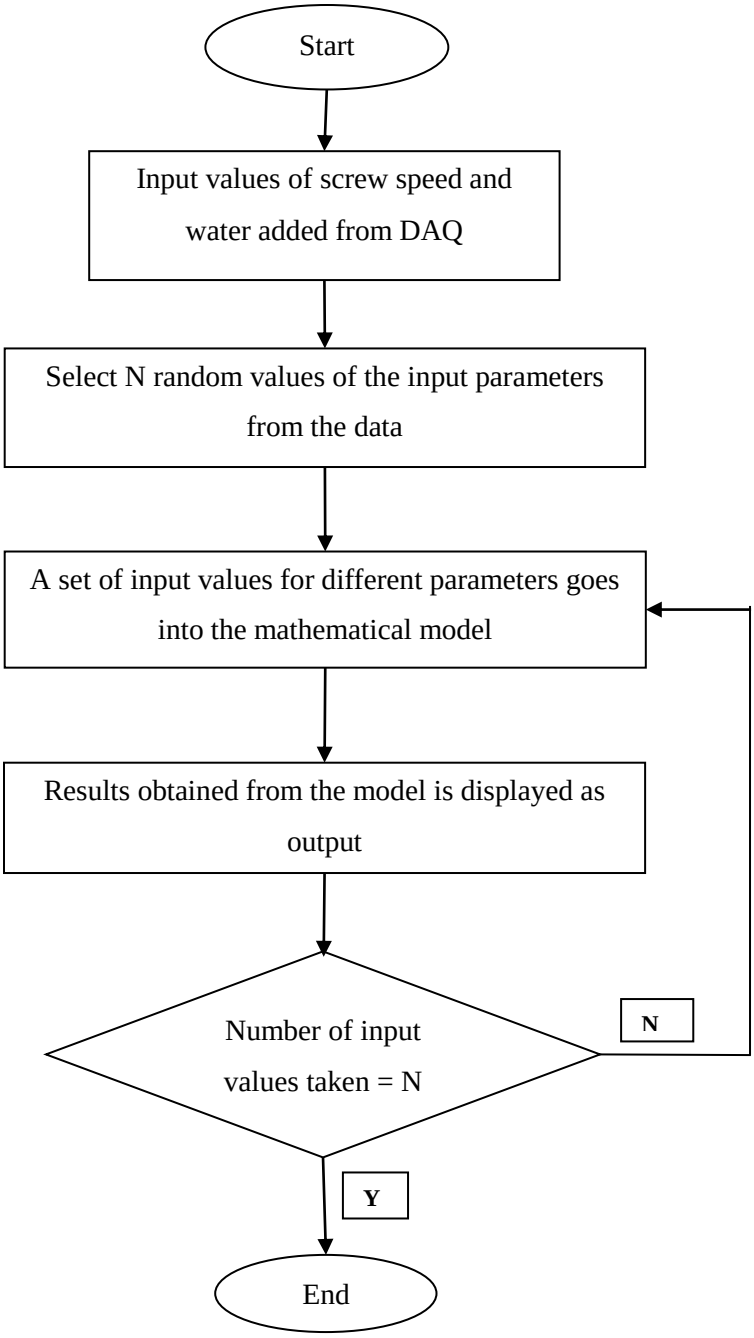

Figure 3-5 Algorithm for stochastic model

3.3 Results

3.3.1 Comparison between predicted and experimental stochastic results

In this study, 20 random values of each input parameter (water added, screw speed) were selected from the DAQ data due to the time constraint. These values were input into the mathematical model and 20 values of expansion ratio were obtained. Each stochastic simulation took about 7-9 hours depending on the computational ability of the computer. The stochastic simulation was carried across all the 6 treatments.

Mean value, Standard Deviation (SD) and Coefficient of Variation (CV) was calculated for the input parameters selected and the output obtained across all 6 treatments. The CV of the sampled input parameters is shown in Table 3-2

Table 3-2 CV of input parameters (moisture content and screw speed)

Treatment	Water added (kg/hr)			Screw speed (RPM)		
	Mean	SD	CV (%)	Mean	SD	CV (%)
M.C. LO, RPM LO	5.8	0.17	2.9	253.9	2.48	0.98
M.C. LO, RPM HI	5.9	0.15	2.6	330	0.28	0.09
M.C. MD, RPM LO	9.9	0.14	1.4	253.3	0.32	0.13
M.C. MD, RPM HI	9.7	0.14	1.5	329.8	0.3	0.09
M.C. HI, RPM LO	14.4	0.15	1.1	253.4	0.35	0.14
M.C. HI, RPM HI	14.6	0.15	1	335.1	0.25	0.07

The output characteristic i.e. ER of the extrudate was obtained from the stochastic model. CV of the predicted ER was obtained using this data. CV of the experimental ER was also calculated. Table 3-3 shows the comparison between the CV of predicted ER and experimental ER.

Table 3-3 Comparison of CV of predicted and experimental expansion ratio

Treatment	Predicted ER			Experimental ER		
	Mean	SD	CV (%)	Mean	SD	CV (%)
M.C. LO, RPM LO	18.6	0.58	3.11	16.9	0.78	4.61
M.C. LO, RPM HI	18.9	0.58	3.07	16.4	0.78	4.74
M.C. MD, RPM LO	6.9	0.15	2.13	8.6	0.4	4.69
M.C. MD, RPM HI	7.5	0.18	2.4	6.9	0.34	4.89
M.C. HI, RPM LO	4.6	0.012	0.26	4.1	0.1	2.54
M.C. HI, RPM HI	4.9	0.012	0.24	3.3	0.12	3.58

The CV of predicted ER for the six treatments was in the range of 0.24 – 3.11 % whereas the CV of experimental ER was in the range of 2.54 - 4.89 %. Predicted CV was bit less compared to Experimental CV because there might be other parameters as well affecting ER.

3.3.2 Sensitivity analysis with respect to input parameters

Using these stochastic simulations, sensitivity analysis was carried out for 3 different input parameters in which 2 input parameters were processing conditions such as water added into the extruder and screw speed and the third input parameter was material property i.e. consistency index. The sensitivity analysis was carried out by varying one input parameter by 10% while keeping other two parameters constant and observing its effect on the expansion ratio.

Table 3-4 Sensitivity analysis of expansion ratio with respect to water added in extruder at M.C. LO, RPM LO

Water added (kg/hr)	Screw speed (RPM)	Consistency index coefficient	ER (Simulated)
5.83	253.9	1	18.7
6.41	253.9	1	16.55
7	253.9	1	12.64

Table 3-5 Sensitivity analysis of expansion ratio with respect to screw speed at M.C. LO, RPM LO

Water added (kg/hr)	Screw speed (RPM)	Consistency index coefficient	ER (Simulated)
5.83	253.9	1	18.7
5.83	279.3	1	18.99
5.83	304.7	1	19.15

Table 3-6 Sensitivity analysis of expansion ratio with respect to consistency index at M.C. LO, RPM LO

Water added (kg/hr)	Screw speed (RPM)	Consistency index coefficient	ER (Simulated)
5.83	253.9	1	18.7
5.83	253.9	1.1	20.5
5.83	253.9	1.2	20.51

Tables 3-4 to 3-6 gives the sensitivity analysis of expansion ratio with respect to water added in extruder, screw speed and consistency index respectively for the treatment M.C. LO, RPM LO. It can be observed that ER decreased with increase in expansion ratio whereas it increased with increase in screw speed and consistency index. A 10% increase in water caused 3.03 relative decrease in ER whereas 10% increase in screw speed caused 0.224 relative increase in ER. For consistency index coefficient, 10% increase caused 0.905 relative increase in ER. This signifies that water added in extruder affects the ER most compared to consistency index coefficient and screw speed.

3.3.3 Sensitivity analysis with respect to variability in input parameters

Variability in input parameters was captured using DAQ data. Figure 3-6 shows that the water added in extruder followed a normal distribution across all the treatments.

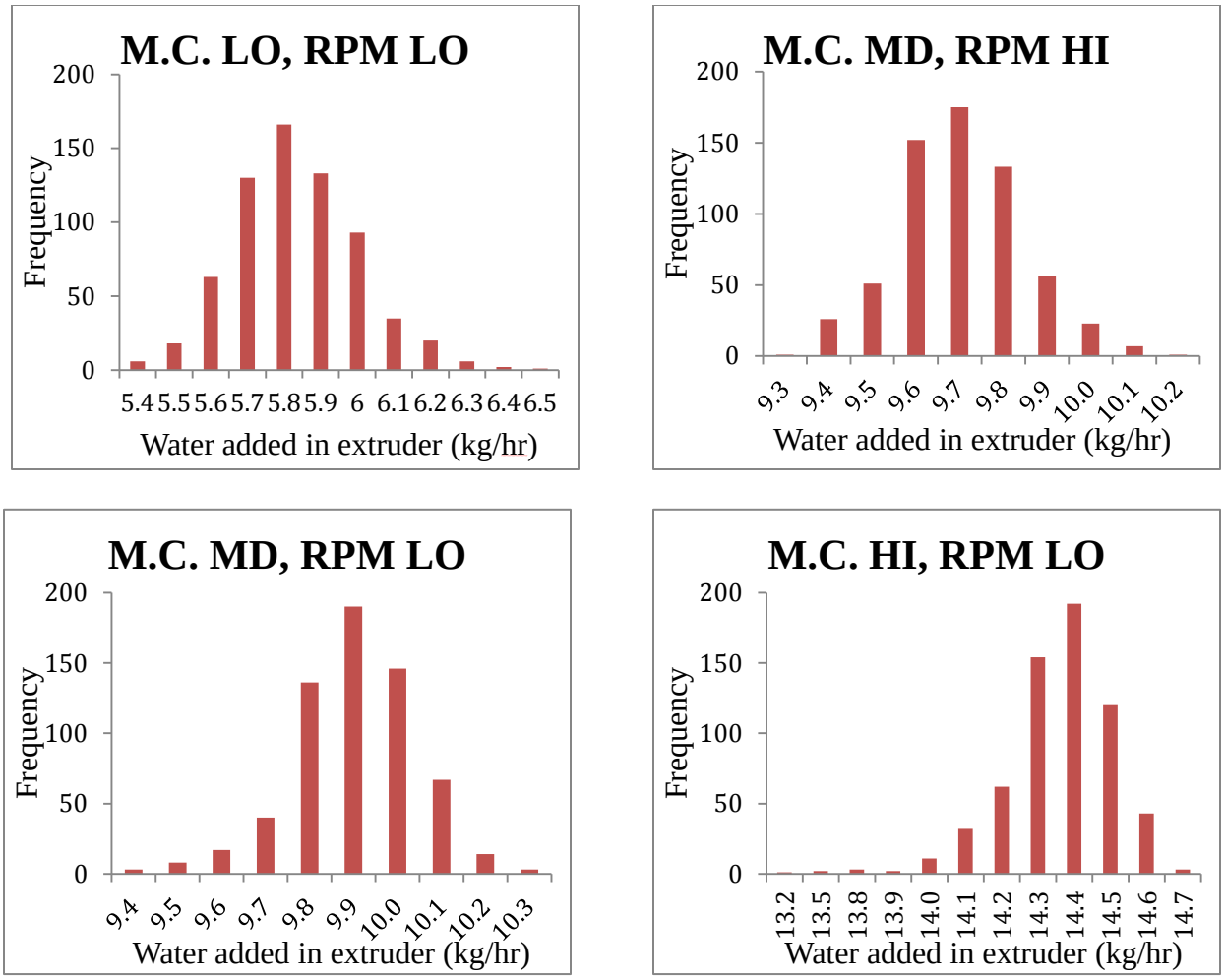

Figure 3-6 Variability in water added in extruder for various treatments

Figure 3-7 shows that there was no specific distribution or pattern in screw speed across all the treatments. Hence the uniform distribution was assumed for screw speed. A uniform distribution was assumed for the third input parameter i.e. consistency index coefficient as well.

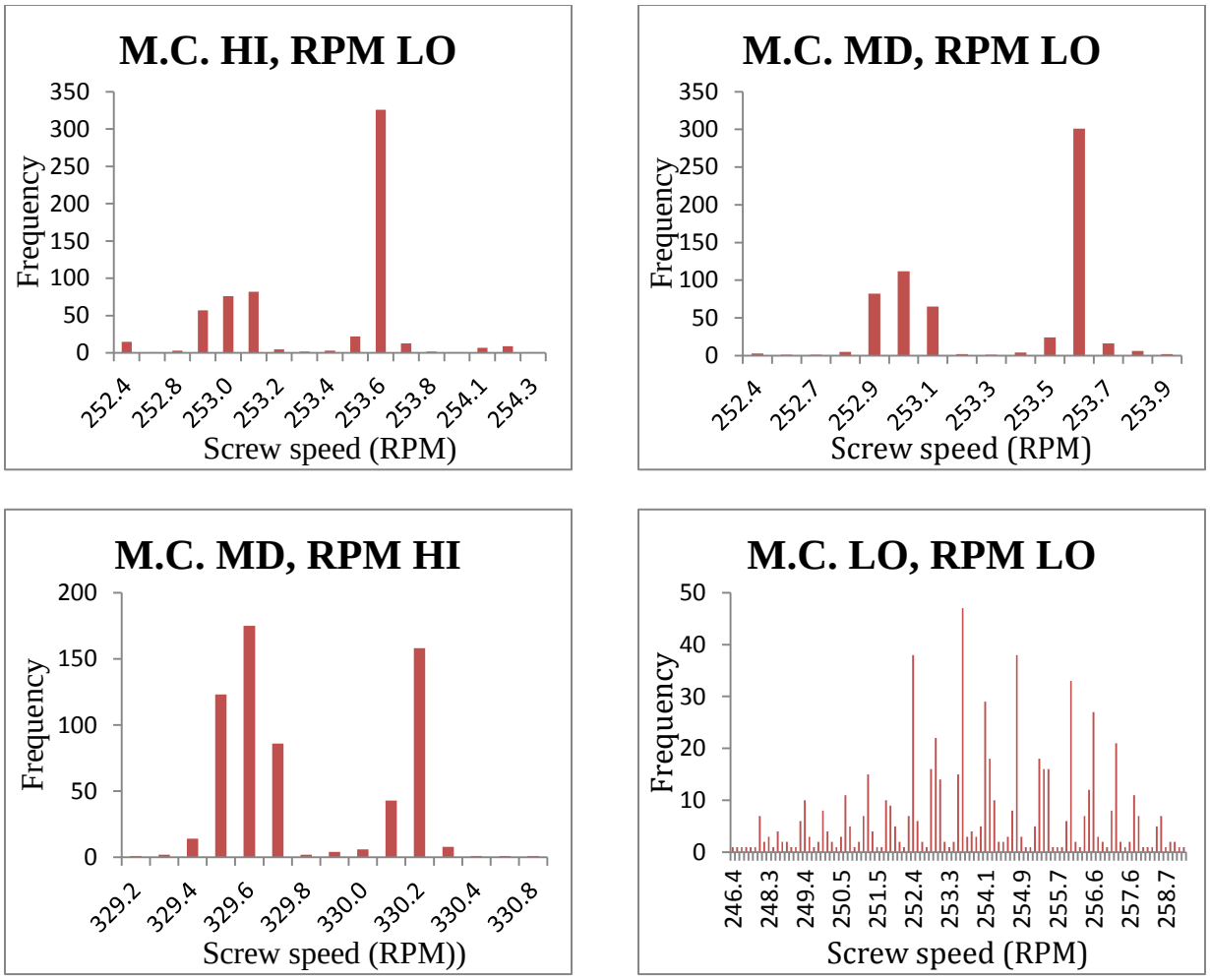

Figure 3-7 Variability in screw speed for various treatments

Tables 3-7 to 3-9 gives the sensitivity analysis of variability in expansion ratio with respect to variability in water added in extruder, screw speed and consistency index respectively for the treatment M.C. LO, RPM LO.

Table 3-7 Sensitivity analysis of variability in expansion ratio with respect to variability in water added in extruder at M.C. LO, RPM LO

Water added in extruder (kg/hr)			Screw speed (RPM)			Consistency index coefficient			ER (simulated)		
Mean	SD	CV(%)	Mean	SD	CV(%)	Mean	SD	CV(%)	Mean	SD	CV(%)
5.83	0.09	**1.5**	253.9	0.25	0.1	1	0.01	1	18.7	0.25	**1.32**
5.83	0.2	**3.5**	253.9	0.25	0.1	1	0.01	1	18.8	0.76	**4.03**
5.83	0.32	**5.5**	253.9	0.25	0.1	1	0.01	1	18.9	1.46	**7.74**

Table 3-8 Sensitivity analysis of variability in expansion ratio with respect to variability in screw speed at M.C. LO, RPM LO

Water added in extruder (kg/hr)			Screw speed (RPM)			Consistency index coefficient			ER (simulated)		
Mean	SD	CV(%)	Mean	SD	CV(%)	Mean	SD	CV(%)	Mean	SD	CV(%)
5.83	0.09	1.5	253.9	0.25	**0.1**	1	0.01	1	18.7	0.25	**1.32**
5.83	0.09	1.5	253.9	5.33	**2.1**	1	0.01	1	18.68	0.26	**1.41**
5.83	0.09	1.5	253.9	10.41	**4.1**	1	0.01	1	18.64	0.27	**1.45**

Table 3-9 Sensitivity analysis of variability in expansion ratio with respect to variability in consistency index coefficient at M.C. LO, RPM LO

Water added in extruder (kg/hr)			Screw speed (RPM)			Consistency index coefficient			ER (simulated)		
Mean	SD	CV(%)	Mean	SD	CV(%)	Mean	SD	CV(%)	Mean	SD	CV(%)
5.83	0.09	1.5	253.9	0.25	0.1	1	0.01	**1**	18.7	0.25	**1.32**
5.83	0.09	1.5	253.9	0.25	0.1	1	0.03	**3**	18.7	0.32	**1.71**
5.83	0.09	1.5	253.9	0.25	0.1	1	0.05	**5**	18.7	0.43	**2.32**

Tables 3-7 to 3-9 gives the sensitivity analysis of variability in expansion ratio with respect to variability in water added in extruder, screw speed and consistency index respectively for the

treatment M.C. LO, RPM LO. It can be observed that increase in CV of any input parameter led to increase in CV of expansion ratio. For 2% CV increase in water added in extruder, relative CV increase in ER was 1.605 whereas 2% CV increase in screw speed and 2% CV increase in consistency index coefficient led to relative CV increase in ER of 0.0325 and 0.25 respectively. This signifies that variability in water added in extruder affects the variability in ER the most compared to screw speed and consistency index coefficient.

In the past, little work has been done on the uncertainty and sensitivity analysis of the food processes. Though Feyissa et al. (2012) studied the uncertainty and sensitivity analysis for mass and heat transfer in a contact baking process; they did not validate the model. Hence, this study was the first one to validate the stochastic model of the food process. Feyissa et al. (2012) determined how the temperature and water content change due to uncertainty in the value of the parameters and identified the relative impact of uncertain parameters on model predictions and ranked the parameters according to their impact. The identification of influential parameters is useful in further refining the model as it gives the idea of which parameters to be measured precisely or should be estimated from experimental data. They found that the evaporation rate constant at the evaporation temperature and thermal conductivity parameter are very important for temperature prediction liquid diffusion coefficient is very important for the prediction of the liquid water concentration.

In non-food industry, Mejlholm et al (2014) developed a stochastic model for simultaneous growth of Listeria monocytegenes and lactic acid bacteria and validated the model from naturally contaminated samples of cold-smoked Greenland halibut and cold-smoked salmon. They studied the effect of 12 environmental parameters and microbial contamination. They used gamma

distribution for some parameters and normal distribution for some parameters from experimental collected data and obtained comparable predictions for stochastic model.

3.4 References

Beck, J.V. & Arnold, K.J. (2007). Parameter estimation in engineering and science, Rev. ed. New York: Wiley.

Campolongo, F. & Saltelli, A. (1997). Sensitivity analysis of an environmental model and application of different analysis methods. Reliability Engineering & System Safety, 57 (1), 49–69.

Cariboni, J., Gatelli, D., Liska, R. & Saltelli, A. (2007). The role of sensitivity analysis in ecological modelling. Ecological Modeling, 203 (1–2), 167–182.

Dolan, K.D. & Mishra, D.K. (2013). Parameter estimation in food science. Annual Review in Food Science and Technology, 4, 401-422.

Ellwein, L.M., Tran, H.T., Zapata, C., Novak, V. & Olufsen, M.S. (2008). Sensitivity analysis and model assessment: mathematical models for arterial blood flow and blood pressure. Cardiovascular Engineering, 8(2), 94–108.

Feyissa, A.H., Gernaey, K.V., & Nissen, J.A. (2012). Uncertainty and sensitivity analysis: Mathematical model of coupled heat and mass transfer for a contact baking process. Journal of Food Engineering, 109, 281-290.

Helton, J.C., Davis, F.J., 2003. Latin hypercube sampling and the propagation of uncertainty in analyses of complex systems. Reliability Engineering & System Safety 81 (1), 23–69.

Mejlholm, O., Boknaes, N. & Dalgaard P. (2014). Development and validation of a stochastic model for potential growth of Listeria monocytogenes in naturally contaminated lightly preserved seafood, Food Microbiology. (Still in press)

Ratto, M., Young, P.C., Romanowicz, R., Pappenberger, F., Saltelli, A. & Pagano, A. (2007). Uncertainty, sensitivity analysis and the role of data based mechanistic modeling in hydrology. Hydrology and Earth System Sciences, 11 (4), 1249–1266.

Saisana, M., Saltelli, A. & Tarantola, S. (2005). Uncertainty and sensitivity analysis techniques as tools for the quality assessment of composite indicators. Journal of the Royal Statistical Society Series A-Statistics in Society, 168, 307–323.

Saltelli, A., Ratto, M., Tarantola, S. & Campolongo, F. (2005). Sensitivity analysis for chemical models. Chemical Reviews, 105 (7), 2811–2827.

Sin, G., Gernaey, K.V. & Lantz, A.E. (2009). Good modeling practice for PAT applications: Propagation of input uncertainty and sensitivity analysis. Biotechnology Progress, 25 (4), 1043–1053.

Sobol, I.M. (2001). Global sensitivity indices for nonlinear mathematical models and their Monte Carlo estimates. Mathematics and Computers in Simulation, 55 (2001), 271–280.

Vergnes, B. & Berzin, F. (2006). Modeling of reactive systems in twin screw extrusion: challenges and applications. Comptes Rendus Chimie, 9, 1409-1418.

Wong, S.Y., Zhou, W. & Hua, J. (2006). Robustness analysis of a CFD model to the uncertainties in its physical properties for a bread baking process. Journal of Food Engineering, 77 (4), 784–791.

Chapter 4 - Conclusions and Future Work

4.1 Conclusions

A deterministic mathematical model was developed for the behavior of flow inside the extruder to simulate pressure, temperature and energy profiles inside the extruder. In spite of so many assumptions, predicted values of temperature, pressure and specific mechanical energy were in good agreement with experimental values.

A deterministic mathematical model for the expansion and shrinkage of bubbles after the extrudate exits from the die was developed and it was coupled with the mathematical model of flow behavior inside the extruder to simulate dynamics of cell structure and obtain end product characteristics such as expansion ratio and cellular architecture parameters (cell size and wall thickness). The model helped in understanding the process of extrusion of biopolymer melts at the fundamental level. Even though, predicted and experimentally obtained results of expansion ratio and maximum expansion ratio showed a good fit; the cellular architecture parameters i.e. cell size and cell wall thickness were statistically different for predicted and experimentally obtained results at level 0.05 suggesting that further work needs to be done in microscopic model. This can be due to the high nucleation density used (27500 bubbles/ cm^3 of unexpanded melt) which causes very low cell wall thickness due to the high number of bubbles. A proper nucleation density and rheological correlation for viscosity is important for studying the dynamics of the bubble and cell wall thickness needs to be further investigated.

A stochastic model was developed and to study the effect of variability of operating conditions (screw speed, water injection) and material properties (consistency coefficient) on the variability of the end product characteristics. This model was also used to conduct sensitivity analysis for understanding which raw material and process characteristics contribute most to product

variability. Sensitivity analysis showed that the water added in extruder affects the expansion ratio the most compared to screw speed and consistency index coefficient.

4.2 Future work

Some future research can involve improving the model prediction for cell wall thickness and average cell size by refining the input parameters for bubble number density and initial cell radius. Phenomenon of coalescence was neglected in the model. Coalescence can be included in the model as it leads to decrease in number of bubbles and results in higher cell size and cell wall thickness as well. The model can be further improved by using different viscosity equations for viscosity inside the extruder and after the product exits the die. The viscosity equations could be different due to the differences in the shear rate inside the extruder and during the bubble growth. The shear rate inside the extruder is very high, whereas after the extrudate exits the die, the shear rate rapidly approaches zero due to free-surface flow.

Further work can also be done on sensitivity analysis at different processing conditions. The sensitivity analysis was done at M.C. LO, RPM LO. The effect of the processing conditions on the end product characteristics may vary at different processing conditions. Sensitivity analysis of other input parameters like feed rate, ambient temperature etc. can be done in order to know which parameter affects the end product the most.

4.2.1 Sample calculations

Phenomenon of coalescence was neglected in the model. Coalescence can be included in the model as it leads to decrease in number of bubbles and results in higher cell size and cell wall thickness as well.

Treatment: M.C. LO, RPM LO

Average cell size R (Experimental) = 655 microns

If 1 cm^3 of expanded product is completely filled with bubbles (fully packed assumption)

Number of bubbles in 1 cc of expanded product = $\frac{1}{(\frac{4}{3}\pi R^3)} = \frac{1}{(\frac{4}{3}\pi(655)^3)}$ = ~850

Sectional expansion ratio (Experimental) = 16.94

Longitudional expansion ratio (Experimental) = 0.627

Overall expansion ratio (Experimental) = 16.94 * 0.627 = 10.62

Number of bubbles in 1 cc of unexpanded melt = 850*10.62 = ~9000

As the coalescence phenomenon is assumed, it is assumed that 9000 bubbles/cm^3 of unexpanded melt coalesce to form 850 bubbles/cm^3 in the expanded product.

Initial radius of the bubble R_o = 100 microns

Initial bubble density N_{cell} = 9000 bubbles/cm^3 of unexpanded melt

Initial domain radius L_o = 285 microns

Final radius of the bubble R = 655 microns

Let us assume that the final domain radius is L

The volume of the solid in the bubble remains the same after expansion

$$\frac{4}{3}\pi(L_o^3 - R_o^3) * 9000 = \frac{4}{3}\pi(L^3 - R^3) * 850$$

$$(285^3 - 100^3) * 9000 = (L^3 - 655^3) * 850$$

$$L = 801.8 \text{ microns}$$

Final cell wall thickness = 801.8 – 655 = 146.8 microns

Final cell wall thickness (experimental) = 136.6 microns

It can be observed that the cell wall thickness obtained from calculations (146.8) was very near to the experimental cell wall thickness (136). This effect is due to coalescence.

Expansion ratio = $\frac{850*\frac{4}{3}\pi*L^3}{9000*\frac{4}{3}\pi*L_o^3} = \frac{850*801.8^3}{9000*285^3}$ = 2.1

But it can be observed that the expansion ratio obtained from calculations (2.1) was very less compared to the experimental expansion ratio (16.94).

Hence, this needs to be further investigated.